Geochronological and Geochemical Effects of Zircon Chemical Abrasion: Insights from Single-Crystal Stepwise Dissolution Experiments

Alyssa J. McKanna[1], Blair Schoene[1], and Dawid Szymanowski[1,2]

[1]Princeton University, Department of Geosciences, Princeton, New Jersey 08544, USA
[2]Institute of Geochemistry and Petrology, ETH Zurich, 8092 Zurich, Switzerland

Correspondence: Alyssa J. McKanna (ajmckanna@gmail.com)

Abstract

Chemical abrasion in hydrofluoric acid (HF) is routinely applied to zircon grains prior to U-Pb dating by isotope dilution thermal ionization mass spectrometry (ID-TIMS) to remove radiation-damaged portions of grains affected by Pb loss. Still, many chemically abraded datasets exhibit evidence of residual Pb loss. Here we test how the temperature and duration of chemical abrasion affects zircon U-Pb and trace element systematics in a series of 4-hour, single-crystal stepwise dissolution experiments at 180 °C and 210 °C. Microtextural data for the zircon samples studied is presented in a complementary paper by McKanna et al. (2023). We find that stepwise dissolution at 210 °C is more effective at eliminating U, common Pb (Pb_c), and light rare earth element (LREE) enriched material affected by open system behavior; reduces the presence of leaching-induced artefacts that manifest as reverse discordance; and produces more consistent and concordant results in zircon from the three rocks studied. We estimate that stepwise dissolution in three 4 h steps is roughly equivalent to a single ~8 h leaching step due to the insulating properties of the PTFE sleeve in the Parr pressure dissolution vessel, whereas traditionally labs utilize a single 12-hour leaching step. We conclude that a single 8 h leaching step at 210 ˚C should remove Pb loss effects in the majority of zircon and that this can be used as an effective approach for routine analysis. Further, we calculate time-integrated alpha doses for leachates and residues from measured radionuclide concentrations to investigate: 1) the alpha dose of the material dissolved at the two leaching conditions, and 2) the apparent minimum alpha dose required for Pb loss susceptibility: ≥ 6×10^{17} α/g.

1. Introduction

Zircon U-Pb geochronology by isotope dilution thermal ionization mass spectrometry (ID-TIMS) has played a pivotal role in constraining the timing and tempo of processes on Earth from the Hadean to the Pleistocene. Zircon is a remarkable chronometer, in part because crystalline zircon is exceptionally chemically and physically durable. The zircon structure, however, can accumulate radiation damage over time. Radiation damage is principally caused by alpha recoil events in the ^{238}U, ^{235}U, and ^{232}Th decay series and the spontaneous fission of ^{238}U (Ewing et al., 2003; Meldrum et al., 1998; Weber, 1990). Radiation-damaged zircon can lose Pb and less commonly U, violating the basic requirement of geochronology that neither parent nor daughter isotopes are lost through time except through radioactive decay (Geisler et al., 2002). Fortunately, the dual $^{206}Pb/^{238}U$ and $^{207}Pb/^{235}U$ decay schemes provide a self-check mechanism

Deleted: ,2
Deleted: 3
Deleted: 2Los Alamos National Lab, Los Alamos, New Mexico 87545, USA¶
Deleted: 3
Deleted: Zürich
Deleted: Zürich
Deleted: lanl.gov
Deleted: To better understand the causes of Pbloss in zircon,
Deleted: w
Deleted:
Deleted: estimates
Deleted: determine
Deleted: for
Deleted: to occur
Deleted: We conclude that a single 8 h leaching step at 210 ˚C should yield crystallization ages in the majority of zircon and that this can be used as an effective approach for routine analysis. However, Ultimately, the effectiveness of any chemical abrasion protocol will be sample-dependent. By framing Pb loss and zircon solubility in terms of alpha dose,however, workers can better tailor the chemical abrasion process to specific zircon samples to improve the accuracy and precision of U-Pb results.
Deleted: 238U/

by which open system behavior can be identified in zircons older than several hundred Ma (Mezger and Krogstad, 1997; Corfu, 2013). In the Phanerozoic, however, the dual decay system becomes less effective at recognizing Pb-loss, since the trajectory of Pb-loss follows concordia, and the precision of $^{207}Pb/^{235}U$ dates is also lower than corresponding $^{206}Pb/^{238}U$ dates due to the lower isotopic abundance of ^{235}U and consequently ^{207}Pb (Corfu, 2013; Schoene, 2014).

In a seminal study, Mattinson (2005, 2011) – building off the previous findings of Krogh and Davis (1975) and Todt and Büsch (1981) – demonstrated that the most radiation-damaged portions of zircon can be effectively removed by hydrofluoric acid (HF) through a series of stepwise dissolution experiments on multi-grain aliquots. He showed that early leaching steps sampled high-U material with discordant U-Pb dates, while later leaching steps sampled low-U residues unaffected by open-system behavior. Mattinson (2005, 2011) further established that partially annealing zircon samples prior to leaching helps to minimize the unwanted elemental and isotopic fractionation effects that plagued earlier leaching attempts (Davis & Krogh, 2000; Todt & Büsch, 1981). These experimental findings revolutionized the field of zircon U-Pb geochronology by allowing scientists to attain meaningful geochronological results from previously unusable zircon affected by open-system behavior. Air abrasion – the pre-treatment technique previously used to improve U-Pb concordance by removing crystal rims which tend to be more exposed to alteration (Krogh, 1981) – was largely abandoned. Today, a variation of Mattison's approach – termed chemical abrasion – is applied to virtually all zircon grains prior to ID-TIMS U-Pb isotopic analysis. In this variation, zircon crystals are annealed at 800 °C to 1200 °C for 36 h to 60 h and then leached in concentrated HF at 180 °C to 210 °C for 10 h to 18 h prior to dissolution and isotopic analysis (Mundil et al., 2004; Huyskens et al., 2016; Widmann et al., 2019).

The decrease in sample size from multi-grain aliquots to portions of single crystals and the concurrent increase in analytical precision in TIMS over the past half-century (e.g., Schoene, 2014) demands a critical re-evaluation of the chemical abrasion technique and the accuracy of the U-Pb ages that the Earth science community has come to rely on. Many studies have now shown that chemically abraded zircon samples often still exhibit residual Pb-loss. This challenge is widely recognized in the ID-TIMS U-Pb community and has prompted investigations into the effects of different annealing and leaching conditions on geochronological outcomes (Huyskens et al., 2016; Widmann et al., 2019), new statistical approaches for evaluating over-dispersed U-Pb datasets (Keller, 2023), and microstructural studies of chemically abraded zircon (McKanna et al., 2023).

We build on the earlier work of Mattinson (2005, 2011) and present a series of new stepwise dissolution experiments performed at the single-crystal scale. We evaluate the effects of stepwise chemical abrasion at 180 °C and 210 °C on zircon U-Pb and trace element systematics in three zircon samples – AS3, SAM-47, and KR18-04 – which span a range of crystallization ages, geological settings, and radiation damage densities. These zircons come from the same sample aliquots as studied by McKanna et al. (2023) in their recent microstructural investigation of zircon dissolution which presents a unique opportunity to integrate zircon microtextures, geochronology, and geochemistry.

Deleted: C

Deleted: $^{238}U/^{206}Pb$

Deleted: shorter radioactive half-life of ^{235}U and

Formatted: Superscript

Formatted: Superscript

Deleted: e

Deleted: (thought to be high in U) and improve U-Pb concordance (Krogh, 1981)

Deleted: new

2. Methods

Zircon samples were annealed in quartz crucibles at 900 °C for 48 h in air in a box furnace prior to the start of the experiments. Annealed grains were mounted in epoxy, polished, and imaged by cathodoluminescence (CL) or backscattered electron (BSE) imaging using a XL30 FEG scanning electron microscope equipped with a mini-Gatan CL detector and a semiconductor BSE detector housed at the PRISM Imaging and Analysis Center at Princeton University. Images of dated zircon crystals are presented in Fig. S1, Fig. S2, and Fig. S3.

The stepwise partial dissolution protocol outlined here is very similar to that of Keller et al., (2019, their Fig. 1). Crystals were plucked from their epoxy mounts, rinsed in 30% HNO_3, and individually transferred to 200 µL PFA microcapsules for partial dissolution in ~100 µL of concentrated HF. Microcapsules were loaded into a PTFE-lined Parr pressure dissolution vessel with 5 mL moat HF and placed in a box oven set to 180 °C or 210 °C for a period of 4 h. At the 4 h mark, the pressure vessel was removed from the oven and placed in front of a fan to cool to room temperature.

The microcapsules were then removed from the pressure vessel and the leachate (the dissolved zircon-HF mixture) from each microcapsule was transferred to a clean 7 mL PFA beaker using a pipette. A fresh, acid-cleaned pipette tip was used for each sample transfer. Approximately 100 µL of 6N HCl was added to the residue (the remaining undissolved zircon) in the microcapsule, and the microcapsule was capped and placed on the hotplate for 1 h. The 6N HCl was then pipetted off the residue and added to the 7 mL PFA beaker with the sample leachate. The residue was then sequentially rinsed in the microcapsule using a pipette with 3N HCl, 6N HCl, 30 % HNO_3, and concentrated HF. These rinses were discarded. About 100 µL of fresh concentrated HF was then added to each residue for the second round of step leaching. In total, samples were partially dissolved in a series of three 4-h leaching steps generating a L1, L2, and L3 leachate for each zircon crystal.

After the L3 leachate was collected, the residue was again rinsed with acid and ~100 µL of fresh HF was added to the microcapsule. Each residue was spiked with the EARTHTIME ^{205}Pb-^{233}U-^{235}U tracer (Condon et al., 2015; McLean et al., 2015) and dissolved in a Parr pressure dissolution vessel in a box oven at 210 °C for 48 to 60 h. Each leachate was spiked with the same tracer, capped, and placed on the hot plate for the same duration. Both leachates and residues were then dried down on the hot plate. Residues were redissolved in ~100 µL of 6N HCl in the Parr pressure vessel in the box oven at 180 °C overnight, and leachates were redissolved in ~100 µL of 6N HCl on an 80 °C hot plate overnight. Afterward, all residues and leachates were dried down on the hot plate and redissolved in 3N HCl in preparation for ion exchange chromatography. This procedure was modified slightly for half of the KR18-04 zircon samples treated at 210 °C to evaluate whether the incomplete dissolution of fluoride salts was causing unwanted U-Pb elemental fractionation effects. For these samples, after each HF leachate was collected, zircon residues were dried down completely on the hot plate before the addition of ~100 µL of 6N HCl. Microcaps were then transferred back to the Parr pressure vessel and redissolved at 180 °C overnight in the box oven. The 6N HCl liquid was then pipetted off the

Deleted: Representative images of AS3, SAM-47, and KR18-04 crystals can be found in McKanna et al. (2023) Fig. 3 and Fig. 4. …

Deleted: the

Deleted: step-leached

Deleted: a protocol change could

Deleted: mitigate

Deleted: as suggested by Mattinson (2005) with the goal of eliminating U-loss caused by the incomplete dissolution of fluoride salts. …

residue and added to the sample's HF leachate in the 7 mL PFA beaker. This procedure was repeated for the L2 and L3 leachates. All other steps remained the same.

PTFE columns were prepared with 50 µL of Eichrom AG1-X8 anion exchange resin, cleaned, and equilibrated. U-Pb ion exchange chemistry followed the protocol established by Krogh (1973) and modified by Schoene et al. (2010) for the collection of trace elements. Combined U and Pb fractions were dried down with trace 0.05 M H_3PO_4 and loaded onto a zone-refined Re filament with a Si-gel emitter (Gerstenberger and Haase, 1997) for isotopic analysis on one of the two IsotopX Phoenix TIMS at Princeton University. Pb isotopes were measured on either the Daly/photomultiplier detector or ATONA Faraday system (Szymanowski and Schoene, 2020), and U isotopes were measured as oxides on Faraday cups with 10^{12} Ω resistors or on the ATONA Faraday system. Mass fractionation of Pb isotopic analyses was corrected for with factors specific to each detector system, derived from a compilation of in-run values measured in samples spiked with the EARTHTIME ^{202}Pb-^{205}Pb-^{233}U-^{235}U tracer using the known $^{202}Pb/^{205}Pb$ ratio of the tracer. Mass fractionation of U isotopic analyses was corrected using the known $^{233}U/^{235}U$ ratio of the tracer. Tripoli and ET-Redux software (Bowring et al., 2011; McLean et al., 2011) were used for processing isotopic data and error propagation, assuming a sample $^{238}U/^{235}U$ ratio of 137.818 ± 0.045 (2σ) (Heiss et al., 2012). All reported $^{206}Pb/^{238}U$ and $^{207}Pb/^{206}Pb$ dates are calculated using the decay constants of Jaffey et al., (1971) and Th-corrected assuming a magma Th/U ratio of 3.5. Reported uncertainties reflect 2σ analytical uncertainties. Common Pb corrections assume a composition equivalent to the blank.

Major and trace element analyses were made using a Thermo Scientific iCap-Q inductively coupled plasma mass spectrometer (ICPMS) at Princeton University following the procedure developed by Schoene et al. (2010), with analytical parameters described in O'Connor et al. (2022). U concentrations were calculated from Th concentrations measured by ICPMS and the Th/U ratio estimated from radiogenic ^{208}Pb and the $^{206}Pb/^{238}U$ age assuming concordance between the U-Pb and Th-Pb systems.

3. Geologic setting, sample description, and previous geochronology

3.1. AS3

AS3 zircons are from an anorthosite from the Duluth Complex of northern Minnesota, USA which formed during the Mesoproterozoic North American Midcontinent Rift (46°45'43.4" N, 92°09'32.4" W) (Paces & Miller, 1993; Miller et al., 2002; Schmitz et al., 2003; Swanson-Hysell et al., 2019, 2020). The Duluth Complex is a massive layered mafic intrusion. The anorthositic and layered series of the complex were emplaced at ~1096 Ma over a duration <1 m.y. (Swanson-Hysell et al., 2020). The voluminous magmatism that formed the Duluth Complex is attributed to decompression melting due to lithospheric extension occurring atop an upwelling mantle plume (Swanson-Hysell et al., 2020). Rifting in the region ceased at ~1084 Ma (Swanson-Hysell et al., 2019). Thermochronology data from the Minnesota River Valley in southern Minnesota suggest that rocks in the region have sat at near-surface temperature conditions since the Neoproterozoic (Guenthner et al., 2013; McDannell et al., 2022).

Deleted: again

Deleted: &

Deleted: in

Formatted: Not Highlight

Deleted: double-spiked

Formatted: Not Highlight

Formatted: Superscript

Formatted: Not Highlight

Formatted: Superscript, Not Highlight

Formatted: Not Highlight

Formatted: Superscript, Not Highlight

Formatted: Not Highlight

Deleted: ;

Deleted: for

Deleted: the

Deleted: correction

Deleted: used

Formatted: Not Highlight

Formatted: Not Highlight

Formatted: Not Highlight

Formatted: Not Highlight

Formatted: Not Highlight

Formatted: Not Highlight

Formatted: Not Highlight

Deleted: The percent zircon dissolved is calculated using Zr abundances: (Zr_{step}/Zr_{total}) × 100. LREE-indices (LREE-I) quantify LREE-enrichment in zircon which can reflect chemical alteration or sample contamination. The lower the LREE-I, the higher the LREE-enrichment. LREE-I is calculated as [Dy]/[Nd] + [Dy]/[Sm] following Bell et al., (2016).

Deleted: ¶
3. Background and results¶
¶
3.1 AS3 ¶

Deleted: 1.1

Deleted: and and

Deleted: s

Deleted: magmatic

The AS3 sample studied is the same as that of Takehara et al. (2018). The rock sample is composed of plagioclase, amphibole, clinopyroxene, and ilmenite with minor K-feldspar, apatite, zircon, and baddeleyite. Partially chloritized amphiboles, altered plagioclase, and zeolite veins indicate that this sample of AS3 has interacted with low-temperature hydrothermal fluids as previously described (Takehara et al., 2018). Zircon grains are large and occur as orange-to-orangish brown tabular prisms or anhedral shards. Grains are fractured and often have large melt inclusions elongated parallel to the *c*-axis. Crystals exhibit concentric and convolute zonation patterns, and many grains are hydrothermally altered (Fig. S1) (McKanna et al., 2023; Takehara et al., 2018). Altered grains and grains with inclusions were included in the experiments to evaluate how well geochemical data traces the dissolution of inclusions and altered material. Raman data indicate that grains have accumulated high radiation damage densities with equivalent alpha doses of 2×10^{17} to $>1\times10^{19}$ α/g with significant intracrystalline variations in radiation damage (McKanna et al., 2023).

Paces and Miller (1993) presented the first U-Pb geochronological data for AS3 zircon. These authors found that six multi-grain aliquots of air-abraded zircon crystals produced concordant ID-TIMS U-Pb dates and assigned the sample a weighted-mean $^{207}Pb/^{206}Pb$ age of 1099.1 ± 0.5 Ma (2σ). Schmitz et al. (2003) later conducted additional ID-TIMS U-Pb isotopic analysis on individual air-abraded AS3 zircon. The authors found that several crystals produced discordant dates affected by recent Pb loss. Twelve concordant analyses yielded a concordia age of 1099.1 ± 0.2 Ma (2σ). Eight grains from the same sample were later analyzed by chemical abrasion ID-TIMS by Schoene et al. (2006). The authors annealed grains at 900 °C for 60 h and chemically abraded them in an HF-HNO_3 mixture at 180 °C for 12 to 14 h. Residues produced concordant dates with weighted mean $^{206}Pb/^{238}U$ and $^{207}Pb/^{206}Pb$ ages of 1095.9 ± 0.2 Ma and 1098.6 ± 0.3 (2σ) assuming a zircon $^{238}U/^{235}U$ ratio of 137.88. Recalculating from published isotope ratios (Schoene et al., 2006) and assuming an updated zircon $^{238}U/^{235}U$ of 137.818 ± 0.045 (2σ) (Heiss et al., 2012) in the age equation yields a $^{207}Pb/^{206}Pb$ age of 1097.7 ± 0.3 (2σ). Age differences between these and previous results were attributed by the authors to differences in tracer calibration, which had been redone as part of Schoene et al. (2006). Takehara et al., (2018) later demonstrated that zircons from a different sample of AS3 collected from the same sample locality are strongly affected by alteration; sensitive high-resolution ion microprobe (SHRIMP) analyses showed that altered zones yielded normally discordant U-Pb analyses; were enriched in incompatible trace elements including LREEs, Ca, Mn, Fe, Al, Li, and K; and depleted in Zr and Si.

3.2 SAM-47

SAM-47 is an Archean (~3.32 - 3.29 Ga) granodiorite from the Corunna Downs Granitic Complex of the Emu Pools Supersuite in the eastern Pilbara Craton (21°24'29.01" S, 119°46'21.03" E) (Barley and Pickard, 1999; Smithies et al., 2003; Van Kranendonk et al., 2007). The tectonic significance of the dome and keel structures of the eastern Pilbara Craton are a matter of debate (stagnate lid versus mobile lid tectonics), and the region has experienced a multi-phase deformational history (Kloppenburg et al., 2001; MacLennan, 2019; Moore and Webb, 2013).

Deleted: oriented

Deleted: Included and

Deleted: a

Deleted: ¶
3.1.2 Previous geochronology¶

Deleted: producing

Deleted: ting

Deleted: calculated assuming a U ratio of 137.88. Recalculated values assuming a U ratio of 137.818 ± 0.045 (2σ) (Heiss et al., 2012) yields $^{206}Pb/^{238}U$ and $^{207}Pb/^{206}Pb$ ages of 1095.9 ± 0.2 Ma and 1097.7 ± 0.3 (2σ), respectfully. These grains were annealed at 900 °C for 60 h and chemically abraded in an HF-HNO_3 mixture at 180 °C for 12 to 14 h.

Deleted: (

Deleted: hydrothermal

Deleted: hydrothermally

Deleted:

Deleted: ,

Deleted: ,

Deleted: ¶

ID-TIMS U-Pb ages for apatite from the Corunna Downs Granitic Complex are ~3.3 Ga which are similar to Ar-Ar ages reported by Kloppenburg (2003). The similarity between the U-Pb and Ar-Ar data suggest rapid cooling through ~460°C following intrusion of the granitoid (MacLennan, 2019). Zircon (U-Th)/He dates for the Owen's Gully diorite from the Mount Edgar Granitic Complex north of the Corunna Downs range from 677.5 ± 36.3 to 815.5 ± 44.6 Ma, suggesting that the eastern craton reached near-surface thermal conditions, where radiation damage can accumulate in zircon, sometime in the Neoproterozoic (Magee et al., 2017). Low-temperature thermochronology data from elsewhere in the Pilbara craton (the northern, central, and western blocks) suggest that the onset of widespread cooling related to basin-development and unroofing varied regionally starting sometime between ~600 and 300 Ma (Morón et al., 2020). Zircon grains separated from SAM-47 are euhedral, brown, translucent, and finely-fractured (Fig. S2). Crystals display fine-scale concentric growth zones, and rims are enriched in actinides and radiation damage relative to cores (McKanna et al., 2023). Raman data suggest that grains have accumulated intermediate-to-high radiation damage densities with equivalent alpha doses ranging from 6×10^{17} to 2×10^{18} α/g (McKanna et al., 2023). There is no previous zircon U-Pb geochronology from this sample, however, Pb-loss is common in similarly aged zircon from the Pilbara craton (MacLennan, 2019).

Deleted: cooling

Deleted: in age

Deleted: and

Deleted: (McKanna et al., 2023).

Deleted: R

Deleted: .

Deleted: for zircon

Deleted:

3.3 KR18-04

KR18-04 zircons come from a Neoproterozoic rhyolite body associated with the glaciolacustrine Konnarock Formation in the Blue Ridge Mountains of Virginia, USA (MacLennan et al., 2020) (36°41'47.95" N, 81°24'22.08" W). The Konnarock Formation is part of a structurally continuous sedimentary sequence deposited in a continental rift environment (Merschat et al., 2014). This sequence unconformably overlies gneisses that are related to the Mesoproterozoic Grenville orogeny. ID-TIMS U-Pb ages for zircon separated from KR18-04 were used to show that glacial sedimentation was occurring at tropical latitudes at ~751 Ma, 30 million years prior to the Sturtian Snowball Earth (MacLennan et al., 2020). The post-depositional history of the region is complex and poorly resolved (Roden, 1991). Zircon fission track dates (T_c = ~205°C) from the Blue Ridge are variably reset by burial reheating and range in age from ~617 Ma to late Paleozoic dates (Naeser et al., 2016). Zircon (U-Th)/He dates (T_c = ~180 °C for crystalline zircon) from the Blue Ridge are contemporaneous with the late-stages of the Alleghenian orogeny indicating that the zircon He chronometer was fully reset by burial reheating and records synorogenic exhumation (Basler et al., 2021).

The KR18-04 rhyolite is crystal-rich with prominent, dominantly euhedral K-feldspar and quartz phenocrysts (MacLennan et al., 2020). Zircon grains separated from KR18-04 are euhedral, pink-orange, transparent, and have few to no inclusions. Grains exhibit concentric zoning in cathodoluminescence images with some faint, broad growth zones (Fig. S3). Raman data suggest that grains have accumulated low-to-intermediate radiation damage densities with equivalent alpha doses ranging from 5×10^{16} to 2×10^{17} α/g (McKanna et al., 2023).

Deleted: minimally included

Deleted: cathodoluminescent

Deleted: (McKanna et al., 2023)

Twelve single-crystal zircon ID-TIMS U-Pb analyses for KR18-04 are presented by MacLennan et al. (2020). Zircon were initially chemically abraded at 185 °C for 12 h. However, since many of

Deleted: ,

these analyses retained significant Pb-loss, the intensity of chemical abrasion was increased to 210 °C for up to 14 h for the remaining samples. The twelve reported $^{206}Pb/^{238}U$ dates – which combine both leaching conditions – range from 753.08 ± 0.33 to 741.21 ± 0.35 Ma. The reported data are statistically over-dispersed for a single population. The authors attribute the spread in ages along concordia and the one discordant analysis to residual Pb-loss (their Fig. S10). The reported eruption age for the sample derived from the eight oldest analyses and determined using a Bayesian Markov Chain Monte Carlo technique is 752.60 +0.12/-0.65 Ma.

4. Results

4.1 U-Pb geochronology

4.1.1 AS3

L1 leachates are strongly affected by Pb-loss, and are enriched in Pb_c derived from inclusions and altered zones (Fig. 1, Table S1). L1 leachates either overlap the concordia curve due to large uncertainties or are normally discordant. L2 and L3 leachates are older than L1 leachates and form a discordia line of analyses that are either normally discordant, concordant, or reversely discordant. The lower intercept ages of the discordia lines are zero-age. L2 and L3 leachates treated at 180 °C are more enriched in Pb_c and ages are more widely dispersed compared to L2 and L3 leachates treated at 210 °C.

Residues treated at 210 °C form a single, concordant age population with a weighted mean $^{206}Pb/^{238}U$ age of 1096.42 ± 0.49 Ma (MSWD = 1.7; Fig. 1). U-Pb ages of residues treated at 180 °C are dispersed along concordia and include reversely discordant analyses, although a cluster of residue analyses yield a weighted mean $^{206}Pb/^{238}U$ age of 1096.29 ± 0.36 Ma (MSWD = 2.3) in agreement with the 210 °C result. Weighted-mean $^{207}Pb/^{206}Pb$ ages for all leachates and residues agree within uncertainty (Fig. 2). The weighted-mean $^{207}Pb/^{206}Pb$ ages obtained for residues are 1097.03 ± 0.63 Ma (MSWD = 1.7) and 1096.64 ± 0.96 Ma (MSWD = 0.48), for the 180°C and 210 °C datasets respectively. The new data agree well with previous geochronology (Schoene et al., 2006).

4.1.2 SAM-47

L1 leachates from both sample sets are strongly affected by Pb-loss (Fig. 3, Table S1). L2 and L3 leachates from the 180 °C experiment are also affected by significant Pb-loss. In contrast, many of the L2 and L3 leachates from the 210 °C experiment are concordant, and the few normally discordant analyses closely approach concordia.

Residues from the 180 °C dataset form a discordia line with two concordant and four normally discordant analyses. The two concordant residues have a weighted-mean $^{206}Pb/^{238}U$ age of 3319.5 ± 1.4 Ma (MSWD = 1.7). All 210 °C residues overlap or closely hug concordia; three concordant residues yield a weighted-mean $^{206}Pb/^{238}U$ age of 3316.1 ± 1.6 Ma (MSWD = 1.0). Upper intercept ages for residues and 210 °C L2 and L3 leachates agree within uncertainty and

Deleted: …oss, the intensity of chemical abrasion was increased to 210 °C for up to 14 h for the remaining samples. The twelve reported $^{206}Pb/^{238}U$ dates – which combine both leaching conditions – range from 753.08 ± 0.33 to 741.21 ± 0.35 Ma. The reported data are statistically over-dispersed for a single population. The authors attribute the spread in ages along cC…ncordia and the one discordant analysis to residual Pb- … [1]

Deleted: 4.1.1 AS3 ¶

Deleted: ID-TIMS U-Pb results for AS3 samples are presented in Fig. 1, Fig. 2, and Table S1. …1 leachates are younger than zircon residues indicating the dissolution of dissolution of material …trongly affected by Pb- …oss. … and are L1 leachates have large age uncertainties due to high amounts of…nriched in Pb_c derived from inclusions and altered zones (Fig. 1, Table S1). Consequently, many large error ellipses overlap the Concordia curve. …1 leachates higher radiogenic to common Pb (Pb^*/Pb_c) ratios and better age precision …ither overlap the concordia curve due to large uncertainties or are normally discordant. L2 and L3 leachates are older than L1 leachates and form a discordia line through …f analyses that are either either …ormally discordant, concordant, or reversely discordant. The upper intercept ages for the discordia lines agree within uncertainty with the weighted mean $^{206}Pb/^{238}U$ age for residues treated at 210 °C. …he lower intercept ages of the discordia lines are zero-age. Ages for … [2]

Deleted: than ages for L2 and L3 leachates treated at 210 °C. The 180 °C leachates also have larger uncertainties due to higher Pb_c contents.

Formatted: Subscript

Deleted: in agreement with previous geochronology (Schoene et al., 2006)… U-Pb ages of residues treated at 180 °C are dispersed along Concordia…oncordia and include reversely discordant analyses, ; …lthough a cluster of residue analyses agree with the 210 °C result …ielding…a weighted mean $^{206}Pb/^{238}U$ age of 1096.29 ± 0.36 Ma (MSWD = 2.3) in agreement with the 210 °C result, but a few analyses are either older or younger. Two of the 180 °C residues are reversely discordant. … Weighted-mean $^{207}Pb/^{206}Pb$ ages for all leachates and residues agree within uncertainty (Fig. 2). The weighted-mean $^{207}Pb/^{206}Pb$ ages obtained for the 180°C and 210 °C …esidues are 1097.03 ± 0.63 Ma (MSWD = 1.7) and 1096.64 ± 0.96 Ma (MSWD = 0.48), for the 180°C and 210 °C datasets respectively. The new data agree well with . These dates are slightly younger than … [3]

Deleted: ID-TIMS U-Pb results for SAM-47 samples are presented in Fig. 2, Fig. 6, and Table S3. …1 leachates from both sample sets are normally discordant resulting in $^{206}Pb/^{238}U$ dates that are >800 Ma. younger than zircon residues, indicating the dissolution of domains …trongly affected by Pb-loss (Fig. 3, Table S1). Although systematically older than L1 leachates, …2 and L3 leach… [4]

Deleted: ¶ … [5]

produce robust MSWDs (Fig. 3). The most precise upper and lower intercept ages are 3321.23 +0.78/-0.71 Ma and 751 ± 140 Ma, respectively. Most $^{207}Pb/^{206}Pb$ dates for L2, L3, and residue samples from the 210 °C experiment agree within uncertainty (Fig. 2). 210 °C residues yield a weighted-mean $^{207}Pb/^{206}Pb$ age of 3321.75 ± 0.63 Ma (MSWD = 0.83) in agreement with upper intercept ages. In contrast, $^{207}Pb/^{206}Pb$ dates from the 180 °C dataset are notably younger, indicating the dissolution of domains affected by ancient Pb-loss. The two concordant 180 °C residue analyses yield a weighted-mean $^{207}Pb/^{206}Pb$ age of 3320.90 ± 0.87 (MSWD = 0.050).

4.1.3 KR18-04

L1 leachates from both sample sets are affected by Pb-loss that occurred at zero-age (Fig. 4, Table S1). L2 leachates from both experiments are concordant and older than zircon residues. L3 leachates are generally concordant, younger than L2 leachates, and slightly older or within uncertainty of zircon residues. Residues from the 180 °C experiment spread along concordia from 758.63 to 752.99 Ma. In contrast, residues from the 210 °C experiment form a tight cluster with a weighted mean $^{206}Pb/^{238}U$ age of 752.49 ± 0.24 Ma (MSWD = 1.1, n=6) in agreement with previous geochronology (MacLennan et al., 2020). This weighted-mean age includes analyses measured on the ATONA which produced more precise U measurements; the batch of samples ran using the traditional amplifiers had very poor U ionization resulting in low quality U measurements. The two 210 °C zircon aliquots that followed slightly different step-leaching protocols as outlined in Methods generated equivalent results.

4.2 Trace element geochemistry

Major and trace element geochemistry data for AS3, SAM-47, and KR18-04 are reported in Table S2. In the 180 °C experiments, leachates for the three zircon samples are enriched in LREE and Pb_c relative to zircon residues (Fig. 5, Fig. 6, and Fig. 7). LREE enrichment is apparent both in chondrite-normalized REE spider diagrams (Fig. S4, Fig. S5, and Fig. S6) and in LREE-indices (LREE-I) (Table S3). LREE-indices – calculated as [Dy]/[Nd] + [Dy]/[Sm] following Bell et al., (2016) – quantify LREE-enrichment in zircon which can reflect chemical alteration or sample contamination. The lower the LREE-I, the higher the LREE-enrichment. In the 210 °C experiments, L1 and some L2 leachates are enriched in LREE and Pb_c, but some L2 and all L3 leachates have LREE and Pb^*/Pb_c compositions similar to residues. Samples' LREE-I and radiogenic to common Pb ratios (Pb^*/Pb_c) are positively correlated.

AS3 leachates are enriched in U relative to residues in the 180 °C dataset (Fig. 8 and Table S3), whereas in the 210 °C dataset only L1 leachates are U-enriched. A similar pattern is seen for KR18-04: L1 and L2 leachates from the 180 °C dataset are enriched in U relative to residues, but only L1 leachates are U-enriched in the 210 °C dataset. Results for SAM-47 differ. Some SAM-47 leachates are marginally enriched in U in the 180 °C dataset, while most leachates from the 210 °C experiment have U compositions similar to residues.

The percent zircon dissolved is calculated from measured Zr abundances: $(Zr_{step}/Zr_{total}) \times 100$ (Fig. 8 and Table S3). This calculation assumes that zircon residues fully dissolve during the final

Deleted: as shown in Fig. 6
Deleted: ¶ ¶
Deleted: R
Deleted: The
Deleted: which agrees well
Deleted: our
Deleted: a
Deleted:
Deleted: event that occurred in the distant past
Deleted: in agreement with the 210 °C results.
Deleted: ID-TIMS U-Pb results for KR18-04 samples are presented in Fig. 9 and Table S5.
Deleted:
Deleted: ; L1 leachates with Pb^*/Pb_c ratios >1 are normally discordant and >150 Ma younger than zircon residues.
Deleted: The lower intercept value for L1 leachates from the 210 °C experiment suggests zero-age Pb-loss.
Deleted: but appreciably
Deleted: The majority of
Deleted: and
Deleted: .
Deleted: Most L3 leachates are either within uncertainty of residue dates or
Deleted: U-Pb analyses of
Deleted: r
Deleted: are
Deleted: C
Deleted: analyses
Deleted: for these
Deleted: low-U zircon
Deleted: ¶ ... [6]
Deleted: L
Deleted: from all the 180 °C experiment
Deleted: ,
Formatted: Not Highlight
Formatted: Not Highlight
Formatted: Subscript
Formatted: Subscript
Deleted: ,
Deleted: and U relative to zircon residues (Fig. 3, Fig. 4 ... [7]

digestion step. For AS3 samples, most dissolution occurred in L1 with progressively smaller fractions dissolved in L2 and L3. The median fraction of the AS3 residue remaining in the 180 °C and 210 °C experiments is ~55 % and ~30 %, respectively. For SAM-47 samples, only 10 to 20 % of the zircon dissolved during leaching at 180 °C, leaving 80 to 90 % of the zircon available for final digestion. At 210 °C, most dissolution in SAM-47 samples occurred in L1 with progressively smaller volumes dissolved in L2 and L3; zircon residues fractions are less than 40 %. For KR18-04 samples, only ~10 to 15 % of zircon dissolved during leaching at 180 °C, leaving residue fractions of ~85 to 95 %. At 210 °C, ~10 °C to 30 % of KR18-04 zircon dissolved during leaching, resulting in 70 to 90 % residue fractions. Percent Pb* ($Pb^*_{step}/Pb^*_{total} \times 100$) calculations mirror results for percent zircon dissolved in all experiments (Fig. 8 and Table S3).

5. Discussion

5.1 Reverse discordance

Reverse discordance and concordant analyses that are older than the samples' interpreted crystallization ages are common in the AS3 and KR18-04 datasets but absent in SAM-47. Concordant analyses that are "too old" can result from either minor U loss or Pb* gain, causing datasets to lie along a discordia line that overlies the concordia curve; for brevity, we will also refer to these analyses as "reversely discordant." Reverse discordance is most common in L2 and L3 leachates, however, a subset of residues from the AS3 and KR18-04 180 °C datasets are also reversely discordant. Three L2 leachates for the Hadean zircon analyzed by Keller et al. (2019) are similarly reversely discordant.

Reverse discordance in zircon stepwise dissolution experiments is generally attributed to leaching-induced experimental artefacts. Early step-leaching efforts yielded U-Pb isotopic variations that swung wildly between normally and reversely discordant from step-to-step (Todt and Büsch, 1981). Mattinson (1994, 2011) later attributed this effect to the authors' specific dissolution and spiking method which caused U and Pb to fractionate between supernate and U-bearing fluoride precipitates. However, later step-leaching experiments using different experimental procedures also exhibited reverse discordance in early leaching steps (Chen et al., 2001; Mattinson, 2005, 2011). Mattinson (2005, 2011) charged that early leaching steps must reflect a mixture of U and Pb from the dissolved zircon volume plus excess Pb* leached from the intact zircon residue. Mattinson (2005, 2011) further demonstrated that annealing samples at temperatures between 800 - 1100 °C prior to chemical abrasion helped to minimize – but not eliminate – leaching-induced artefacts.

Reverse discordance is observed naturally in some untreated zircon (Kusiak et al., 2015; Wiemer et al., 2017; Williams et al., 1984). In such cases, reverse discordance is generally attributed to either the internal redistribution of Pb within a crystal or to external factors such as alteration by hydrothermal fluids (Mattinson et al., 1996). Alpha recoil can displace Pb* from the position of its parent radioisotope by ~30 nm (Ewing et al., 2003; Weber, 1990, 1993). In crystals with fine-scale growth zoning, Pb* produced by a U atom within a high-U zone can be implanted into a nearby low-U zone producing a localized occurrence of excess Pb* in the low-

Deleted: In …or the majority of …S3 samplessamples… most dissolution occurred in L1 the first leaching step …ith progressively smaller volumes …ractions dissolved in L2 and L3. The median fraction of the AS3 zircon mass …esidue ¶ remaining after L3 for…n the 180 °C and 210 °C experiments is ~55 % and , whereas for the 210 °C experiment it is …30 %, respectively. Percent Pb* mirrors results for percent zircon dissolved in both experiments … [8]

Deleted: .¶
¶
4.2.2 SAM-47 ¶
¶
L1, L2, and some L3 leachates from the 180 °C experiment are enriched in LREE and Pb_c relative to zircon residues (Fig. 7, Fig. 8, and Table S4). Some – but not all – leachates from the 180 °C dataset are also marginally enriched in U relative to residues (Fig. 5). The composition of a subset of 180 °C L3 leachates closely approximates that of residues. LREE and Pb_c enrichment is also evident in L1 and some L2 leachates from the 210 °C dataset, whereas most L3 leachates have compositions comparable to residues. Although a few leachates from the 210 °C experiment are relatively enriched in U, many have U compositions similar to residues.¶
¶ … [10]

Formatted … [9]

Deleted: …irrors…results for percent zircon dissolved in both … … [12]

Formatted … [11]

Deleted: 4

Deleted: 4

Deleted: C…ncordia curve; for brevity, we will also refer to these analyses as "reversely discordant." Reverse discordance is most common in L2 and L3 leachates, however, a subset of residues from the AS3 and KR18-04 180 °C experiments … … [13]

Deleted: ,

Deleted: higher-U …issolved zircon volume plus excess Pb* leached from the lower-U … [14]

Deleted: by

U zone (Mattinson et al., 1996). Further, ion imaging and atom probe tomography studies of zircon support the case for nano-to-micro scale Pb redistribution under elevated temperatures and pressures (Kusiak et al., 2015; Peterman et al., 2019, 2021; Reddy et al., 2016). These studies show that unsupported Pb* often forms clusters that are not spatially associated with parent radionuclide growth patterns. However, the exact mechanisms by which Pb* migrates through the zircon structure are poorly understood.

Notably, our SAM-47 zircon does not exhibit reverse discordance suggesting that only some samples are predisposed to leaching-induced artifacts or leaching-exposed natural U-Pb fractionation. A zircon's U-Pb systematics as revealed by stepwise dissolution must therefore reflect its unique compositional characteristics such as the length-scale and magnitude of radionuclide zonation, the extent of Pb loss, or the sample's geological history. AS3 is hydrothermally altered, so a component of the reverse discordance observed could potentially reflect the redistribution of Pb isotopes during hydrothermal alteration (Takehara et al., 2018). Why KR18-04 zircon is susceptible to reverse discordance is less clear. Grains appear unaltered and most compositional zones are broad; however, some grains do have thin, high-U zones that could contribute to the internal redistribution of Pb* (McKanna et al., 2023 their Fig. 4 & 15a). Zircon fission track and (U-Th)/He data from Blue Ridge indicate that the region was thermally affected by burial reheating during the late-Paleozoic Alleghenian Orogeny (Naeser et al., 2016; Roden, 1991). Still, there is no evidence that KR18-04 has experienced an extreme high-temperature deformation event. SAM-47 may lack leaching-induced reverse discordance simply because Pb loss in the sample is so pervasive.

Regardless of the underpinning causes of reverse discordance, this work and that of Mattinson (2005, 2011) demonstrate that increasing the leaching duration and/or temperature helps to eliminate zircon domains affected by open system behavior. These results also highlight that under-leaching samples can produce over-dispersed U-Pb datasets fraught with geologically meaningless analyses. Without the additional context that the 210 °C experiment provides, a researcher could easily interpret the older concordant dates from the 180 °C KR18-04 dataset, for example, as inheritance or prolonged magmatic residence. We stress, however, that our step-wise experiments are under-leached compared to the normal 12 h leaching step used in most labs (see Section 4.3).

5.2 The strengths and limitations of geochemical tools for identifying open-system behavior

Common Pb and LREEs are incompatible in zircon. Mineral and melt inclusions and hydrothermally altered or metamict zones, however, tend to be enriched in LREEs and common Pb (Bell et al., 2016, 2019). Consequently, geochemical indicators such as a sample's LREE-index (LREE-I = [Dy]/[Nd] + [Dy]/[Sm]) and Pb^*/Pb_c (provided demonstrably low laboratory blanks) are useful tools for identifying contamination, hydrothermal alteration, and metamictization. Indeed, our data show that the two variables are generally positively correlated (Fig. 5C, Fig. 6C, and Fig. 7B). Another important geochemical indicator is U concentration – or effective U concentration (eU = U + 0.235 × Th) – which is a measure of the relative radiation damage in a sample.

Deleted:

Deleted: 4

Deleted: 4

Deleted: 8C

Deleted: 11B

Deleted: ; zircon crystals or leachates from the same sample with higher eU have more radiation damage than crystals or leachates with lower eU.

These three geochemical indicators are useful tools for evaluating zircon dissolution. In the 180 °C experiments, L1, L2, and some L3 leachates are enriched in LREE, Pb_c, and U relative to zircon residues. Whereas in the 210 °C experiments, L1 and some L2 leachates are enriched in the three variables, however, some L2 and most L3 leachates have compositions similar to residues.

Micro-X-ray computed tomography data presented by McKanna et al. (2023) for AS3 and SAM-47 zircon show that acid readily accesses crystal cores via fractures to dissolve mineral and melt inclusions and strongly metamict zones during L1 at 180 °C and 210 °C. As such, we interpret the LREE, Pb_c, and U enrichment in L1 leachates to reflect the dissolution of inclusions, metamict material, and – in the case of AS3 – hydrothermally altered zones. We attribute LREE, Pb_c, and U enrichments in later leaching steps to the continued dissolution of soluble radiation-damaged or altered domains. KR18-04 zircon grains are more crystalline and typically lack fractures. Consequently, acid only accesses the cores of some grains, and some inclusions armored by highly crystalline material appear to survive twelve hours of chemical abrasion at 180 °C or 210 °C (McKanna et al., 2023). Consequently, LREE and Pb_c enrichment in L2 and L3 leaching steps could reflect later-stage dissolution of inclusions as well as the continued dissolution of radiation-damaged or altered domains.

Comparing leachate and residue chemistry is extremely effective at illuminating the progress of zircon dissolution. However, stepwise chemical abrasion is a time- and labor-intensive process. The overwhelming majority of zircon ID-TIMS U-Pb studies perform single-step chemical abrasion and discard the leachate. Only the residue is characterized. In an ideal scenario, geochemical indicators such as those described here could be used to support the inclusion or exclusion of anomalously young (or old) analyses from geochronological interpretations. Fig. 9 shows ΔAge (Ma) of residues plotted as a function of a grain's LREE-I, Pb^*/Pb_c, or eU. ΔAge is calculated as the difference between a residue's measured $^{206}Pb/^{238}U$ date and each sample's accepted crystallization age. Negative values for ΔAge reflect Pb loss, while positive values indicate reverse discordance.

Unfortunately, there is no clear correlation between either of the three geochemical indicators and ΔAge in the samples analyzed. Instead, the data suggest that relative enrichments in LREE, Pb_c, and U in residues are not reliable indicators of residual open system behavior. We speculate that the residual zircon affected by open-system behavior is likely volumetrically small compared to the volume of the residual closed-system zircon. Thus, the geochemical signature of the open-system behavior is likely masked by the bulk chemistry of the closed-system residue. Relative enrichments in LREE, Pb_c, and U in residues are likely useful geochemical indicators only if the residual open-system material is proportionally large.

5.3 Leaching temperature and one-step versus stepwise chemical abrasion

Stepwise dissolution at 210 °C out-performed stepwise dissolution at 180 °C for all three zircon samples and produced more consistent, concordant datasets. Leaching at 210 °C dissolved zircon material affected by open-system behavior earlier in the leaching process minimizing the

Deleted: ,

Deleted: in

Deleted: 12

Deleted: 4

frequency and magnitude of normal and reverse discordance compared to the 180 °C experiments (Fig. 1, 2, 3, and 4). The efficacy of the higher leaching temperature is also evident in zircon geochemistry; leaching at 210 °C more efficiently removed zircon material enriched in U, LREE, and Pb_c.

Notably, U-Pb results for AS3 and KR18-04 residues treated by stepwise dissolution at 180 °C are markedly worse than in previous studies (MacLennan et al., 2020; Schoene et al., 2006). Chemical abrasion of AS3 zircon for 12 to 14 h at 180 °C by Schoene et al. (2006) produced concordant, statistically significant weighted mean U-Pb ages without signs of residual Pb-loss or reverse discordance. Those authors used intensive magnetic separation to target diamagnetic zircon without inclusions, whereas this study included altered grains. While some KR18-04 grains treated at 185 °C for 12 h by (MacLennan et al., 2020) exhibited Pb loss, none of their chemically abraded residues were found to be anomalously old or reversely discordant.

These apparent discrepancies beg the question: is stepwise dissolution in three 4 h leaching steps equivalent to a single 12 h leaching step? PTFE has a low thermal conductivity making it an effective insulator. To evaluate how temperature in the PTFE-lined Parr pressure dissolution vessel changes with time, a small hole was drilled through the top of an old PTFE liner. The pressure vessel was assembled as normal minus the rupture and corrosion disks. A type-K thermocouple with an insulated wire was threaded through the top of the pressure vessel and into the center of the PTFE liner. The pressure vessel was then placed in a box furnace at 180 °C or 210 °C. Temperature was monitored using a Perfect Prime thermocouple until the temperature in the liner reached equilibrium with the box furnace. The pressure vessel was then removed from the furnace and placed in front of a fan, and temperature was recorded as the pressure vessel cooled to room temperature.

Results indicate that PTFE is indeed a very effective insulator; the interior of the pressure vessel heats and cools slowly (Fig. 10). It takes 90 to 95 minutes for the interior of the pressure vessel to reach within 20 °C of the target temperature and an additional 30 to 35 minutes to reach within 10 °C of the target temperature. The pressure vessel takes ~90 minutes to cool to room temperature once removed from the oven.

Given the heating ramp up and cool down times for the PTFE-lined pressure dissolution vessel, samples spend only ~2 h of a 4 h leaching step within 10 °C of the target temperature. As such, a sample leached in three consecutive 4 h steps spends ~6 h within 10 °C of the target temperature. Conversely, a sample leached in a single 12 h step spends ~10 h within 10 °C of the target temperature – ~4 h longer than the step-leached sample. Volume loss estimates for KR18-04 further support this conclusion; volume losses for crystals treated by stepwise chemical abrasion (Fig. 8) are lower than volume losses for crystals chemically abraded for a single 12-h step (McKanna et al., 2023; their Fig. 18).

We estimate that our dated residues have been leached for a duration equivalent to a single ~8 h leaching step on the basis of a 10 °C threshold. Given our U-Pb results, we conclude that zircon chemically abraded at 180 °C for a single 8 h step are “undercooked” and will likely

Deleted: Figures
Deleted: 6
Deleted: 7
Deleted: , and 10).
Deleted: hotter
Deleted: ,
Deleted:
Deleted: intense
Deleted: frantzing
Deleted: unincluded,
Deleted: is equivalent to stepwise dissolution in three 4 h leaching steps
Deleted: thermometer
Deleted: near
Deleted: 13
Deleted: the
Deleted: for 12 h
Deleted: leaching
Deleted: estimated
Deleted: Figure
Deleted: 5
Deleted: generally
Deleted: the estimated
Deleted: presented by
Deleted: (
Deleted: for zircon from the same sample aliquot that were chemically abraded for a single 12-h step.
Deleted: On the basis of the 10 °C threshold,
Deleted: w

produce data affected by residual Pb-loss and/or leaching-induced artifacts. Unfortunately, we cannot comment on the efficacy of the routinely practiced 12-hour leaching at 180 ˚C used in many labs, except to say it is likely more effective than the results for residues presented here. Zircon samples chemically abraded at 210 °C for a single 8-h leach are likely to produce geologically meaningful results.

5.4 The relationships between alpha dose, Pb-loss, and zircon dissolution: Moving toward a more predictable model for chemical abrasion

Zircon is an outstanding chronometer because radiogenic Pb is immobile in well crystalline zircon (Cherniak et al., 2009; Cherniak and Watson, 2000). Establishing the alpha dose at which radiogenic Pb can mobilize within the zircon structure would help make Pb-loss more predictable. We calculate three different time-integrated alpha doses for each sample using Eq. 1 where N_A is Avogadro's number; ^{238}U, ^{235}U, and ^{232}Th are concentrations (ppm) determined for leachates and residues; λ values are the respective decay constants; M values are the respective molar masses (g/mol), and t is the chosen damage accumulation interval (Table 1 and Table S3).

Eq. 1

$$\alpha\ \text{dose} = \frac{8 \cdot N_A \cdot {}^{238}U}{M_{238} \cdot 10^6} \cdot (e^{\lambda_{238} t} - 1) + \frac{7 \cdot N_A \cdot {}^{235}U}{M_{235} \cdot 10^6} \cdot (e^{\lambda_{235} t} - 1) + \frac{6 \cdot N_A \cdot {}^{232}Th}{M_{232} \cdot 10^6} \cdot (e^{\lambda_{232} t} - 1)$$

"Total" alpha dose assumes a damage accumulation interval equivalent to a sample's crystallization age. This calculation ignores the possibility of radiation damage annealing. "Present day" alpha dose estimates attempt to take geological annealing into account. Radiation damage anneals at temperatures above ~200 to 300°C on geological timescales (Bernet, 2009; Yamada et al., 2007). The closure temperature for the (U-Th)/He system in crystalline zircon is ~180 °C (Guenthner et al., 2013; Reiners et al., 2004). As such, we use published zircon (U-Th)/He dates or thermal histories derived from zircon (U-Th)/He datasets for the Minnesota River Valley (Guenthner et al., 2013; McDannell et al., 2022), the Eastern Pilbara craton (Magee et al., 2017), and the Virginia Blue Ridge (Basler et al., 2021) to estimate minimum damage accumulation intervals for samples' "present day" alpha doses. Since zircon (U-Th)/He dates for the Eastern Pilbara craton broadly overlap the lower-intercept U-Pb concordia age for SAM-47, we take the lower-intercept age as the damage accumulation interval. Chosen intervals for "present day" alpha doses for AS3, SAM-47, and KR18-04 are 750 Ma, 751 Ma, and 298 Ma, respectively.

"Present day" alpha dose estimates can also be established independently using Raman spectroscopy, since key bands in the zircon Raman spectrum broaden predictably with increasing alpha dose (Nasdala et al., 2001; Palenik et al., 2003). "Present day" alpha doses for AS3 and SAM-47 closely match Raman-based alpha doses (α_r) determined by McKanna et al. (2023) for zircon from the same sample aliquots (Table 1). "Present day" alpha doses for KR18-04 have a similar lower bound but a higher upper bound compared to Raman estimates (McKanna et al., 2023). Most likely, Raman measurements failed to capture volumetrically

Deleted:
Deleted: Zircon samples chemically abraded at 210 °C for a single 8-h leach are more likely to produce geologically meaningful results. …
Deleted: therefore
Deleted: we
Deleted: 4
Deleted:
Deleted:
Deleted: atomic
Deleted: using the radionuclide concentrations determined for leachates and residues (Table 1).
Formatted: Font color: Text 1
Deleted: y ¶
Deleted: ¶
Deleted: ¶
Deleted: c
Deleted: (
Deleted: ,

small, higher-U domains such as the thin concentric dissolution features evident in secondary electron images of KR18-04 residues (McKanna et al., 2023, their Fig. 15a-I reproduced here in Fig. 13b).

The final calculation estimates alpha dose at the time of Pb-loss. Because AS3 and KR18-04 exhibit zero-age Pb-loss, "present day" and "Pb-loss" alpha doses estimates are equivalent. The Pb-loss discord for SAM-47, however, suggests that Pb-loss occurred in the distant geological past at or before 751 ± 140 Ma (Fig. 3C). Therefore, the maximum "Pb-loss" damage accumulation interval is the difference between the sample's upper and lower intercept ages which equates to ~2571 Ma.

Fig. 11 shows the distribution of "Pb-loss" alpha dose estimates for all leachates affected by Pb-loss. Despite vastly different geological settings and ranges in radiation damage densities, leachates affected by Pb-loss exhibit similar alpha dose distributions. The majority have alpha doses that are ≥ 6×10^{17} α/g. We therefore establish this alpha dose as our best estimate for the threshold above which Pb can mobilize within the zircon structure. The mechanism that mobilizes Pb – diffusion, leaching, or recrystallization – is not clear, however, fluids likely play an important role. As such, while zircon with alpha doses above 6×10^{17} α/g may be *susceptible* to Pb loss, not all damaged grains will be affected by open system behavior. Notably, the 6×10^{17} α/g threshold is somewhat lower than the alpha dose – 1×10^{18} α/g – at which zircon material properties such as density begin to change (Ewing et al., 2003; Nasdala et al., 2004). However, the 6×10^{17} α/g threshold is similar to some estimates for the alpha dose at which helium diffusion begins to increase causing the closure temperature for He in zircon to decrease (Anderson et al., 2017, 2020).

For the best geochronological outcomes, chemical abrasion should target zircon material susceptible to Pb-loss, i.e., material with alpha doses above 6×10^{17} α/g. Fig. 12 shows "present day" alpha dose estimates for all leachates and residues from the 180 °C and 210 °C experiments. The apparent differences in alpha dose between the two leaching temperatures reflects the fraction of material dissolved in each step. At 180 °C, smaller volumes of high-U zones dissolve, whereas at 210 °C larger volumes of material including both high-U and medium-U zones dissolve causing average alpha doses to be lower in the 210 °C dataset.

In the 180 °C experiments, the median alpha dose decreases with increasing leaching duration consistent with the expected effects of radiation damage on zircon solubility (Fig. 12). A majority of residues from the 180 °C experiments have alpha doses > 6×10^{17} α/g suggesting that residues may be affected by residual open system behavior in agreement with our U-Pb isotopic results. Evidently, dissolving zircon with lower alpha doses requires longer leaching durations at 180 °C than achieved in this study, which was equivalent to a single 8-hour leach step. In contrast, the median alpha dose for residues as well as L2 and L3 leachates from the 210 °C experiments have alpha doses below the established threshold. Zircon material with alpha doses ≥ 6×10^{17} α/g is thus readily dissolved at short leaching durations at 210 °C.

Deleted: 16b
Deleted:
Deleted: discords
Deleted:
Deleted:
Deleted: 6
Deleted:
Deleted: 14
Deleted:
Deleted:
Deleted:
Formatted: Font: Italic
Deleted: is
Deleted: kinetics
Deleted: ¶
Deleted:
Formatted: Font: +Body (Calibri)
Deleted: with alpha doses ≥ 6 × 10^17 α/g
Deleted: 15
Formatted: Font: +Body (Calibri)
Formatted: Font: +Body (Calibri)
Formatted: Font: +Body (Calibri)
Formatted: Font: +Body (Calibri), Font color: Text 1
Formatted: Font color: Auto
Formatted: Normal (Web)
Deleted: ¶

Framing Pb loss and zircon solubility in terms of alpha dose allows a user to better predict how chemical abrasion might affect a specific zircon dataset. Chemical abrasion is a time-consuming method that is applied to the majority of ID-TIMS U-Pb datasets, but it may be unnecessary for low-alpha dose, inclusion-free zircon. Further, by estimating a sample's "present day" alpha dose distribution, a user can better anticipate how a sample will dissolve (McKanna et al., 2023). For example, if a sample has accumulated a lot of radiation damage like SAM-47, leaching longer than a single 8-h step at 210 °C will likely leave little to no residue for isotopic analysis. Whereas, if a sample has a lower average alpha dose like KR18-04, a longer 210 °C leach is likely safe and potentially more effective.

Determining alpha dose prior to dissolution, however, remains an outstanding challenge. Raman spectroscopy is one method that can be used to estimate alpha dose (Nasdala et al., 2001; Palenik et al., 2003). Alpha dose can also be estimated from laser ablation ICPMS U-Pb data, since laser ablation U-Pb analysis is often used for pre-screening grains for ID-TIMS U-Pb dating. Unfortunately, both methods are time- and resource-intensive. Fig. 13 plots alpha dose as a function of time for different U concentrations. As described above, different time intervals can be selected for damage accumulation depending on the calculation's goal. This figure is a simple visual representation that can help a researcher determine whether or not a sample is likely to be susceptible to Pb loss given a range of possible U concentrations and a rough estimate for the sample's damage accumulation interval.

As highlighted in Fig. 13b, perhaps the most persistent challenge when it comes to tailoring chemical abrasion for a specific zircon dataset are crystal-specific factors such as the spatial distribution and magnitude of intracrystalline variations in radiation damage, inclusions, and fractures which strongly affect how a zircon dissolves as discussed in our companion paper (McKanna et al., 2023). While micro-X-ray computed tomography can visualize inclusions and fractures in zircon in three-dimensions (3D) (McKanna et al., 2023), at present, no method exists for quantifying radiation damage zonation in 3D. Radionuclide zoning explains the inconsistent dissolution behavior evidenced in Fig. 8. For example, the percent zircon dissolved in each leaching step decreases from L1 to L3 for AS3 zircon, remains constant or decreases for SAM-47 zircon, and remains constant or increases for KR18-04 zircon. This inconsistent behavior occurs because the percent zircon dissolved is not only a function of alpha dose, but also 1) the volumetric proportion of zircon with a given alpha dose, and 2) which portions of a crystal are in contact with HF at any given time during the leaching process. Building a comprehensive model for chemical abrasion will ultimately require both geochemical and textural inputs.

6. Conclusions

Single-crystal stepwise dissolution experiments performed at 180 °C and 210°C provide new insights into the geochronological and geochemical effects of chemical abrasion on zircon datasets. Because of the insulating properties of the PTFE-lined pressure dissolution vessel, stepwise dissolution in three 4-h leaching steps is not equivalent to a 12-h single-step chemical abrasion, the method most commonly used by the zircon ID-TIMS U-Pb community. We

Deleted:
Deleted: dissolution
Deleted: better
Deleted: the
Deleted:
Deleted: tailor their
Deleted: approach to a
Deleted: .
Deleted: predict
Deleted: readily a
Deleted: unlikely to have a significant effect
Deleted: ¶
Deleted: ¶
Determining alpha dose prior to dissolution, however, remains an outstanding challenge. Raman spectroscopy is one method that can be used to estimate alpha dose, but Raman is often time- and resource-intensive.
Deleted: 16
Deleted: affected by
Deleted: Chemical abrasion is a time-consuming method that is applied to the majority of ID-TIMS U-Pb datasets, but it may be unnecessary for low-alpha dose, inclusion-free zircon. Further, by estimating a sample's "present day" alpha dose distribution, a user can better predict how readily a sample will dissolve. For example, if a sample has a lot of accumulated radiation damage like SAM-47, leaching longer than a single 8-h step at 210 °C will likely leave little to no residue for isotopic analysis. ... [15]
Deleted: 16b
Deleted: or even a specific zircon crystal is radionucli ... [16]
Deleted: T
Deleted: of radionuclides
Deleted: the
Deleted: intracrystalline variations in
Deleted:
Deleted: strongly
Deleted: the mechanics of
Deleted: dissolution
Deleted: .
Deleted: 5
Deleted: non-pattern
Deleted: ¶ ... [17]
Deleted: 5

estimate that our stepwise dissolution approach is roughly equivalent to 8-h single-step chemical abrasion. Stepwise dissolution at 180 °C produced over-dispersed U-Pb datasets affected by both residual Pb-loss and leaching-induced or leaching-exposed artefacts which present as reverse discordance. Without the context of the 210 °C results, reverse discordance in the 180 °C datasets could easily be mistaken for prolonged crystallization or inheritance and lead to spurious geological interpretations. Longer leaching durations are likely needed to produce robust geochronological datasets at 180 °C.

Stepwise dissolution at 210 °C outperformed the 180 °C experiments by all measures for the three zircon samples analyzed producing more reproducible, concordant results. Ultimately, how a zircon sample responds to any chemical abrasion protocol will be sample-dependent. However, our results suggest that 8-h single-step chemical abrasion at 210 °C may be effective at mitigating Pb-loss and reverse discordance for a wide range of zircon samples. Further study of different zircon samples is needed. Our results, however, clearly demonstrate that leaching durations longer than an 8-h single step are required for chemical abrasion at 180 °C to be effective.

U concentration, Pb^*/Pb_c, and LREE enrichment are useful tools for tracking the dissolution of inclusions and radiation-damaged or altered material during stepwise dissolution. These geochemical indicators, however, are not effective at identifying residual Pb-loss in the zircon residues analyzed.

We attempted to constrain the relationship between Pb-loss and radiation damage by calculating an alpha dose for each leachate based on its measured radionuclide concentration and an estimated damage accumulation interval informed by the sample's geologic history. "Pb-loss" alpha dose estimates suggest that Pb may mobilize within the zircon structure at alpha doses as low as 6×10^{17} α/g. "Present day" alpha dose estimates indicate that many residues treated by stepwise dissolution at 180 °C have alpha doses above the 6×10^{17} α/g threshold, and consequently, many 180 °C residues are affected by residual Pb-loss. The majority of residues treated at 210 °C – and many L2 and L3 leachates – have "present day" alpha doses below this threshold. Grains expected to have accumulated alpha doses < 6×10^{17} α/g based on expected radionuclide concentrations and damage accumulation intervals are unlikely to be affected by Pb-loss and may not require chemical abrasion. However, chemical abrasion may help improve the precision of U-Pb analyses even in low-damage grains by dissolving Pb_c-bearing inclusions. The effectiveness of any chemical abrasion protocol will ultimately be sample-dependent, since zircon dissolution depends not only on a grain's bulk chemistry, but also the spatial distribution and magnitude of intracrystalline variations in radiation damage.

Data availability. All data presented are included in this paper or the Supplement.

Supplement. The supplement related to this article is available online at:

Deleted:

Deleted:

Deleted:

Deleted:

Deleted:

Deleted:

Author contributions. AJM carried out the experiments and wrote the manuscript. All authors – AJM, DS, and BS – contributed to the experiment design and data reduction, interpretation, and presentation.

Competing interests. The contact author has declared that none of the authors has any competing interests.

Disclaimer. Publisher's note: Copernicus Publications remains neutral with regard to jurisdictional claims in published maps and institutional affiliations.

Acknowledgements. Thank you to Mami Takehara of the National Institute of Polar Research in Tokyo, Japan, for providing the hydrothermally altered AS3 zircon crystals used in this study. We would like to thank Fernando Corfu and an anonymous reviewer for their thoughtful feedback that helped to improve this manuscript.

Financial support. This work was supported by research funds provided by the Department of Geosciences at Princeton University granted to Alyssa J. McKanna as part of her Harry Hess Postdoctoral Fellowship.

Review statement.

References

Anderson, A. J., Hodges, K. V., & van Soest, M. C. (2017). Empirical constraints on the effects of radiation damage on helium diffusion in zircon. *Geochimica et Cosmochimica Acta*, *218*, 308–322. https://doi.org/10.1016/j.gca.2017.09.006

Anderson, A. J., van Soest, M. C., Hodges, K. V., & Hanchar, J. M. (2020). Helium diffusion in zircon: Effects of anisotropy and radiation damage revealed by laser depth profiling. *Geochimica et Cosmochimica Acta*, *274*, 45–62. https://doi.org/10.1016/j.gca.2020.01.049

Barley, M. E., & Pickard, A. L. (1999). 41-62 An extensive, crustally-derived. In *Precambrian Research* (Vol. 96).

Basler, L. C., Baughman, J. S., Fame, M. L., & Haproff, P. J. (2021). Spatially variable syn- and post-Alleghanian exhumation of the central Appalachian Mountains from zircon (U-Th)/He thermochronology. *Geosphere*, *17*(4), 1151–1169. https://doi.org/10.1130/GES02368.1

Bell, E. A., Boehnke, P., Barboni, M., & Harrison, T. M. (2019). Tracking chemical alteration in magmatic zircon using rare earth element abundances. *Chemical Geology*, *510*, 56–71. https://doi.org/10.1016/j.chemgeo.2019.02.027

Bell, E. A., Boehnke, P., & Harrison, T. M. (2016). Recovering the primary geochemistry of Jack Hills zircons through quantitative estimates of chemical alteration. *Geochimica et Cosmochimica Acta*, *191*, 187–202. https://doi.org/10.1016/j.gca.2016.07.016

Bernet, M. (2009). A field-based estimate of the zircon fission-track closure temperature. *Chemical Geology*, *259*(3–4), 181–189. https://doi.org/10.1016/j.chemgeo.2008.10.043

Bowring, J. F., McLean, N. M., & Bowring, S. A. (2011). Engineering cyber infrastructure for U-Pb geochronology: Tripoli and U-Pb-Redux. *Geochemistry, Geophysics, Geosystems*, *12*(6). https://doi.org/10.1029/2010GC003479

Chen, F., Siebel, W., & Satir, M. (2001). Zircon U-Pb and Pb-isotope fractionation during stepwise HF acid leaching and geochronological implications. In *Chem. Geol* (Vol. 172). www.elsevier.com/locate/chemgeo

Cherniak, D. J., & Watson, E. B. (2000). Pb diffusion in zircon. *Chemical Geology*, *172*, 5–24. www.elsevier.comrlocaterchemgeo

Cherniak, D. J., Watson, E. B., & Thomas, J. B. (2009). Diffusion of helium in zircon and apatite. *Chemical Geology*, *268*(1–2), 155–166. https://doi.org/10.1016/j.chemgeo.2009.08.011

Condon, D. J., Schoene, B., McLean, N. M., Bowring, S. A., & Parrish, R. R. (2015). Metrology and traceability of U-Pb isotope dilution geochronology (EARTHTIME Tracer Calibration Part I). *Geochimica et Cosmochimica Acta*, *164*, 464–480. https://doi.org/10.1016/j.gca.2015.05.026

Corfu, F. (2013). A century of U-pb geochronology: The long quest towards concordance. In *Bulletin of the Geological Society of America* (Vol. 125, Issues 1–2, pp. 33–47). https://doi.org/10.1130/B30698.1

Davis, D. W., & Krogh, T. E. (2000). Preferential dissolution of 234 U and radiogenic Pb from a-recoil-damaged lattice sites in zircon: implications for thermal histories and Pb isotopic fractionation in the near surface environment. In *Chemical Geology* (Vol. 172). www.elsevier.comrlocaterchemgeo

Ewing, R. C., Meldrum, A., Wang, L., Weber, W. J., & Corrales, L. R. (2003). Radiation Effects in Zircon. *Reviews in Mineralogy and Geochemistry*, *53*(1), 387–425. https://doi.org/10.2113/0530387

Geisler, T., Pidgeon, R. T., van Bronswijk, W., & Kurtz, R. (2002). Transport of uranium, thorium, and lead in metamict zircon under low-temperature hydrothermal conditions. *Chemical Geology*, *191*, 141–154. www.elsevier.com/locate/chemgeo

Gerstenberger, H., & Haase, G. (1997). A highly effective emitter substance for mass spectrometric Pb isotope ratio determinations. In *Chemical Geology* (Vol. 136).

Guenthner, W. R., Reiners, P. W., Ketcham, R. A., Nasdala, L., & Giester, G. (2013). Helium diffusion in natural zircon: radiation damage, anisotropy, and the interpretation of zircon (U-TH)/He thermochronology. *American Journal of Science*, *313*(3), 145–198. https://doi.org/10.2475/03.2013.01

Heiss, J., Condon, D. J., McLean, N., & Noble, S. R. (2012). 238U/235U Systematics in Terrestrial Uranium-Bearing Minerals. *Science*, *335*(6076), 1610–1613.

Huyskens, M. H., Zink, S., & Amelin, Y. (2016). Evaluation of temperature-time conditions for the chemical abrasion treatment of single zircons for U-Pb geochronology. *Chemical Geology*, *438*, 25–35. https://doi.org/10.1016/j.chemgeo.2016.05.013

Jaffey, A. H., Flynn, K. F., Glendenin, L. E., Bentley, W. C., & Essling, A. M. (1971). Precision Measurement of Half-Lives and Specific Activities of 235U and 238U. *Physical Review C*, *4*(5), 1889–1906. https://doi.org/10.1103/PhysRevC.4.1889

Keller, B. (2023). Technical Note: Pb-loss-aware Eruption/Deposition Age Estimation. *GChron*, *Preprint*. https://doi.org/10.5194/gchron-2023-9

Formatted: German (Switzerland)

Formatted: German (Switzerland)

Keller, B. C., Boehnke, P., Schoene, B., & Harrison, T. M. (2019). Stepwise chemical abrasion-isotope dilution-thermal ionization mass spectrometry with trace element analysis of microfractured Hadean zircon. *Geochronology*, *1*(1), 85–97. https://doi.org/10.5194/gchron-1-85-2019

Kloppenburg, A. (2003). *Structural evolution of the Marble Bar Domain, Pilbara granite-greenstone terrain, Australia : the role of Archaean mid-crustal detachments = Structurele evolutie van het Marble Bar Domein, Pilbara graniet-groensteen terrein, Australie : de rol van Archaeische decollements in de middenkorst* [PhD Dissertation]. Utrecht University.

Kloppenburg, A., White, S. H., & Zegers, T. E. (2001). Structural evolution of the Warrawoona Greenstone Belt and adjoining granitoid complexes, Pilbara Craton, Australia: implications for Archaean tectonic processes. In *Precambrian Research* (Vol. 112). www.elsevier.com/locate/precamres

Krogh, T. E. (1973). A low-contamination method for hydrothermal decomposition of zircon and extraction of U and Pb for isotopic age determinations. *Geochimica et Cosmochimica Acta*, *37*, 485–494.

Krogh, T. E. (1981). Improved accuracy of U-Pb zircon ages by the creation of more concordant systems using an air abrasion technique. *Geochimica et Cosmochimico Acta*, *46*, 637–649.

Kusiak, M. A., Dunkley, D. J., Wirth, R., Whitehouse, M. J., Wilde, S. A., & Marquardt, K. (2015). Metallic lead nanospheres discovered in ancient zircons. *Proceedings of the National Academy of Sciences of the United States of America*, *112*(16), 4958–4963. https://doi.org/10.1073/pnas.1415264112

MacLennan, S. A. (2019). *Temporal constraints on Archean crustal geodynamics and Neoproterozoic glaciation* [PhD Dissertation]. Princeton University.

MacLennan, S. A., Eddy, M. P., Merschat, A. J., Mehra, A. K., Crockford, P. W., Maloof, A. C., Southworth, C. S., & Schoene, B. (2020). Geologic evidence for an icehouse Earth before the Sturtian global glaciation. *Science Advances*, *6*(24). https://doi.org/10.1126/sciadv.aay6647

Magee, C. W., Danišík, M., & Mernagh, T. (2017). Extreme isotopologue disequilibrium in molecular SIMS species during SHRIMP geochronology. *Geoscientific Instrumentation, Methods and Data Systems*, *6*(2), 523–536. https://doi.org/10.5194/gi-6-523-2017

Mattinson, J. M. (1994). Mineralogy and Petrology A study of complex discordance in zircons using step-wise dissolution techniques. *Contributions to Mineralogy and Petrology*, *116*, 117–129.

Mattinson, J. M. (2005). Zircon U-Pb chemical abrasion ("CA-TIMS") method: Combined annealing and multi-step partial dissolution analysis for improved precision and accuracy of zircon ages. *Chemical Geology*, *220*(1–2), 47–66. https://doi.org/10.1016/j.chemgeo.2005.03.011

Mattinson, J. M. (2011). Extending the Krogh legacy: development of the CA–TIMS method for zircon U–Pb geochronologyThis article is one of a series of papers published in this Special Issue on the theme of *Geochronology* in honour of Tom Krogh. *Canadian Journal of Earth Sciences*, *48*(2), 95–105. https://doi.org/10.1139/E10-023

Mattinson, J. M., Graubard, C. M., Parkinson, D. L., & McClelland, W. C. (1996). U-Pb Reverse Discordance in Zircons: The Role of Fine-Scale Oscillatory Zoning and Sub-Micron Transport

Formatted: German (Switzerland)

Deleted: Maclennan, S. A., Eddy, M. P., Merschat, A. J., Mehra, A. K., Crockford, P. W., Maloof, A. C., Southworth, C. S., & Schoene, B. (2020). *Geologic evidence for an icehouse Earth before the Sturtian global glaciation*. http://advances.sciencemag.org/¶

of Pb. In A. Basu & S. Hart (Eds.), *Earth Processes: Reading the Isotopic Code* (pp. 355–370). AGU. https://doi.org/10.1029/GM095p0355

McDannell, K. T., Keller, C. B., Guenthner, W. R., Zeitler, P. K., & Shuster, D. L. (2022). Thermochronologic constraints on the origin of the Great Unconformity. *Proceedings of the National Academy of Sciences*, *119*(5). https://doi.org/10.1073/pnas.2118682119

McKanna, A. J., Koran, I., Schoene, B., & Ketcham, R. A. (2023). Chemical abrasion: the mechanics of zircon dissolution. *Geochronology*, *5*(1), 127–151. https://doi.org/10.5194/gchron-5-127-2023

McLean, N. M., Bowring, J. F., & Bowring, S. A. (2011). An algorithm for U-Pb isotope dilution data reduction and uncertainty propagation. *Geochemistry, Geophysics, Geosystems*, *12*(6). https://doi.org/10.1029/2010GC003478

McLean, N. M., Condon, D. J., Schoene, B., & Bowring, S. A. (2015). Evaluating uncertainties in the calibration of isotopic reference materials and multi-element isotopic tracers (EARTHTIME Tracer Calibration Part II). *Geochimica et Cosmochimica Acta*, *164*, 481–501. https://doi.org/10.1016/j.gca.2015.02.040

Meldrum, A., Boatner, L. A., Weber, W. J., & Ewing, R. C. (1998). Radiation damage in zircon and monazite. *Geochimica et Cosmochimica Acta*, *62*(14), 2509–2520.

Merschat, A. J., Southworth, S., McClellan, E., Tollo, R. P., Rankin, D. W., Hooper, S., & Bauer, S. (2014). Key structural and stratigraphic relationships from the northeast end of the Mountain City window and the Mount Rogers area, Virginia–North Carolina–Tennessee. In *Elevating Geoscience in the Southeastern United States: New Ideas about Old Terranes—Field Guides for the GSA Southeastern Section Meeting, Blacksburg, Virginia, 2014* (pp. 63–101). Geological Society of America. https://doi.org/10.1130/2014.0035(03)

Mezger, K., & Krogstad, E. J. (1997). Interpretation of discordant U-Pb zircon ages: An evaluation. *Journal of Metamorphic Geology*, *15*(1), 127–140. https://doi.org/10.1111/j.1525-1314.1997.00008.x

Miller, J. S., Matzel, J. E. P., Miller, C. F., Burgess, S. D., & Miller, R. B. (2007). Zircon growth and recycling during the assembly of large, composite arc plutons. *Journal of Volcanology and Geothermal Research*, *167*(1–4), 282–299. https://doi.org/10.1016/j.jvolgeores.2007.04.019

Moore, W. B., & Webb, A. A. G. (2013). Heat-pipe Earth. *Nature*, *501*(7468), 501–505. https://doi.org/10.1038/nature12473

Morón, S., Kohn, B. P., Beucher, R., Mackintosh, V., Cawood, P. A., Moresi, L., & Gallagher, S. J. (2020). Denuding a Craton: Thermochronology Record of Phanerozoic Unroofing From the Pilbara Craton, Australia. *Tectonics*, *39*(9). https://doi.org/10.1029/2019TC005988

Mundil, R., Ludwig, K. R., Metcalfe, I., & Renne, P. R. (2004). Age and Timing of the Permian Mass Extinctions: U/Pb Dating of Closed-System Zircons. *Science*, *305*, 1760–1762. www.sciencemag.org

Naeser, C. W., Naeser, N. D., Newell, W. L., Southworth, S., Edwards, L. E., & Weems, R. E. (2016). Erosional and depositional history of the Atlantic passive margin as recorded in detrital zircon fission-track ages and lithic detritus in Atlantic Coastal plain sediments. *American Journal of Science*, *316*(2), 110–168. https://doi.org/10.2475/02.2016.02

Formatted: German (Switzerland)

Formatted: German (Switzerland)

Nasdala, L., Reiners, P. W., Garver, J. I., Kennedy, A. K., Stern, R. A., Balan, E., & Wirth, R. (2004). Incomplete retention of radiation damage in zircon from Sri Lanka. *American Mineralogist*, *89*, 219–231.

Nasdala, L., Wenzel, M., Vavra, G., Irmer, G., Wenzel, T., & Kober, B. (2001). Metamictisation of natural zircon: Accumulaton versus thermal annealing of radioactivity-induced damage. *Contributions to Mineralogy and Petrology*, *141*(2), 125–144. https://doi.org/10.1007/s004100000235

O'Connor, L., Szymanowski, D., Eddy, M. P., Samperton, K. M., & Schoene, B. (2022). A red bole zircon record of cryptic silicic volcanism in the Deccan Traps, India. *Geology*, *50*(4), 460–464. https://doi.org/10.1130/G49613.1

Paces, J. B., & Miller, J. D. (1993). Precise U-Pb ages of Duluth Complex and related mafic intrusions, northeastern Minnesota: geochronological insights to physical, petrogenetic, paleomagnetic, and tectonomagmatic processes associated with the 1.1 Ga Midcontinent Rift system. *Journal of Geophysical Research*, *98*(B8). https://doi.org/10.1029/93jb01159

Palenik, C. S., Nasdala, L., & Ewing, R. C. (2003). Radiation damage in zircon. *American Mineralogist*, *88*, 770–781.

Peterman, E. M., Reddy, S. M., Saxey, D. W., Fougerouse, D., Snoeyenbos, D. R., & Rickard, W. D. A. (2019). Nanoscale processes of trace element mobility in metamorphosed zircon. *Contributions to Mineralogy and Petrology*, *174*(11). https://doi.org/10.1007/s00410-019-1631-1

Peterman, E. M., Reddy, S. M., Saxey, D. W., Fougerouse, D., Zakaria Quadir, M., & Jercinovic, M. J. (2021). Trace-element segregation to dislocation loops in experimentally heated zircon. *American Mineralogist*, *106*(12), 1971–1979. https://doi.org/10.2138/am-2021-7654

Reddy, S. M., van Riessen, A., Saxey, D. W., Johnson, T. E., Rickard, W. D. A., Fougerouse, D., Fischer, S., Prosa, T. J., Rice, K. P., Reinhard, D. A., Chen, Y., & Olson, D. (2016). Mechanisms of deformation-induced trace element migration in zircon resolved by atom probe and correlative microscopy. *Geochimica et Cosmochimica Acta*, *195*, 158–170. https://doi.org/10.1016/j.gca.2016.09.019

Reiners, P. W., Spell, T. L., Nicolescu, S., & Zanetti, K. A. (2004). Zircon (U-Th)/He thermochronometry: He diffusion and comparisons with 40Ar/39Ar dating. *Geochimica et Cosmochimica Acta*, *68*(8), 1857–1887. https://doi.org/10.1016/j.gca.2003.10.021

Roden, M. K. (1991). Apatite Fission-Track Thermochronology of the Southern Appalachian Basin: Maryland, West Virginia, and Virginia. *The Journal of Geology*, *99*(1), 41–53. https://doi.org/10.1086/629472

Schmitz, M. D., Bowring, S. A., & Ireland, T. R. (2003). *Evaluation of Duluth Complex anorthositic series (AS3) zircon as a U-Pb geochronological standard: New high-precision isotope dilution thermal ionization mass spectrometry results*. https://doi.org/10.1016/S0016-7037(00)00200-X

Schoene, B. (2014). U–Th–Pb Geochronology. In *Treatise on Geochemistry* (pp. 341–378). Elsevier. https://doi.org/10.1016/B978-0-08-095975-7.00310-7

Schoene, B., Crowley, J. L., Condon, D. J., Schmitz, M. D., & Bowring, S. A. (2006). Reassessing the uranium decay constants for geochronology using ID-TIMS U-Pb data. *Geochimica et Cosmochimica Acta*, *70*(2), 426–445. https://doi.org/10.1016/j.gca.2005.09.007

Formatted: German (Switzerland)

Schoene, B., Latkoczy, C., Schaltegger, U., & Günther, D. (2010). A new method integrating high-precision U-Pb geochronology with zircon trace element analysis (U-Pb TIMS-TEA). *Geochimica et Cosmochimica Acta*, *74*(24), 7144–7159. https://doi.org/10.1016/j.gca.2010.09.016

Smithies, R. H., Champion, D. C., & Cassidy, K. F. (2003). Formation of Earth's early Archaean continental crust. *Precambrian Research*, *127*(1–3), 89–101. https://doi.org/10.1016/S0301-9268(03)00182-7

Swanson-Hysell, N. L., Hoaglund, S. A., Crowley, J. L., Schmitz, M. D., Zhang, Y., & Miller, J. D. (2020). Rapid emplacement of massive Duluth Complex intrusions within the North American Midcontinent Rift. *Geology*, *49*(2), 185–189. https://doi.org/10.1130/G47873.1

Swanson-Hysell, N. L., Ramezani, J., Fairchild, L. M., & Rose, I. R. (2019). Failed rifting and fast drifting: Midcontinent Rift development, Laurentia's rapid motion and the driver of Grenvillian orogenesis. *Bulletin of the Geological Society of America*, *131*(5–6), 913–940. https://doi.org/10.1130/B31944.1

Szymanowski, D., & Schoene, B. (2020). U–Pb ID-TIMS geochronology using ATONA amplifiers. *Journal of Analytical Atomic Spectrometry*, *35*(6), 1207–1216. https://doi.org/10.1039/D0JA00135J

Takehara, M., Horie, K., Hokada, T., & Kiyokawa, S. (2018). New insight into disturbance of U-Pb and trace-element systems in hydrothermally altered zircon via SHRIMP analyses of zircon from the Duluth Gabbro. *Chemical Geology*, *484*, 168–178. https://doi.org/10.1016/j.chemgeo.2018.01.028

Todt, W. A., & Büsch, W. (1981). U-Pb investigations on zircons from pre-Variscan gneisses-I. A study from the Schwarzwald, West Germany. *Geochimica et Cosmochimica Acta*, *45*, 1789–1801.

Van Kranendonk, M. J., Hugh Smithies, R., Hickman, A. H., & Champion, D. C. (2007). Review: Secular tectonic evolution of Archean continental crust: interplay between horizontal and vertical processes in the formation of the Pilbara Craton, Australia. In *Terra Nova* (Vol. 19, Issue 1, pp. 1–38). https://doi.org/10.1111/j.1365-3121.2006.00723.x

Weber, W. J. (1990). Radiation-induced defects and amorphization in zircon. *J. Mater. Res.*, *5*(11), 2687–2697. http://journals.cambridge.org

Weber, W. J. (1993). Alpha-Decay-Induced Amorphization in Complex Silicate Structures. *Journal of the American Ceramic Society*, *76*(7), 1729–1738. https://doi.org/10.1111/j.1151-2916.1993.tb06641.x

Widmann, P., Davies, J. H. F. L., & Schaltegger, U. (2019). Calibrating chemical abrasion: Its effects on zircon crystal structure, chemical composition and U–Pb age. *Chemical Geology*, *511*, 1–10. https://doi.org/10.1016/j.chemgeo.2019.02.026

Wiemer, D., Allen, C. M., Murphy, D. T., & Kinaev, I. (2017). Effects of thermal annealing and chemical abrasion on ca. 3.5 Ga metamict zircon and evidence for natural reverse discordance: Insights for U[sbnd]Pb LA-ICP-MS dating. *Chemical Geology*, *466*, 285–302. https://doi.org/10.1016/j.chemgeo.2017.06.019

Williams, I. S., Compston, W., Black, L. P., Ireland, T. R., & Foster, J. J. (1984). Contributions to Mineralogy and Petrology Unsupported radiogenic Pb in zircon: a cause of anomalously high Pb-Pb, U-Pb and Th-Pb ages. In *Contrib Mineral Petrol* (Vol. 88).

Formatted: German (Switzerland)

Yamada, R., Murakami, M., & Tagami, T. (2007). Statistical modelling of annealing kinetics of fission tracks in zircon; Reassessment of laboratory experiments. *Chemical Geology*, *236*(1–2), 75–91. https://doi.org/10.1016/j.chemgeo.2006.09.002

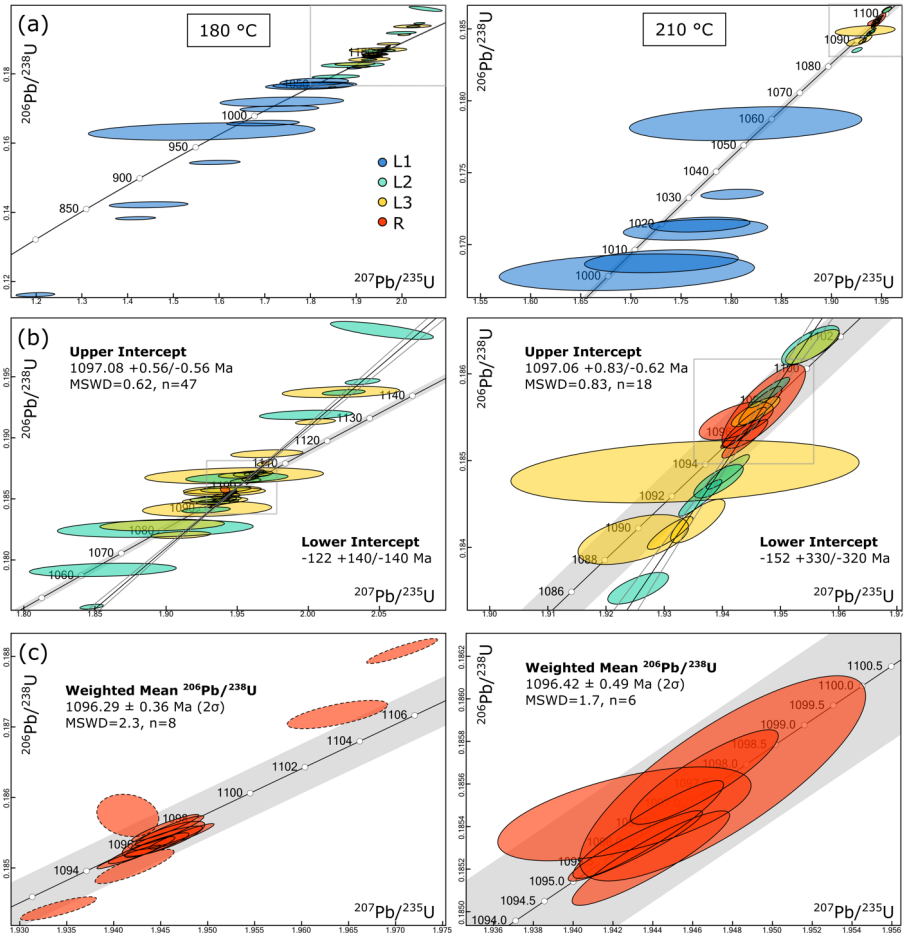

Figure 1. U-Pb concordia diagrams for the 180 °C (left) and 210 °C (right) AS3 experiments. **(a)** All data are depicted except for L1 leachates with Pb^*/Pb_c values < 1. **(b)** Close up of L2, L3, and R data. **(c)** Close up of zircon residue data. Ellipses with dashed borders were excluded from the weighted-mean $^{206}Pb/^{238}U$ age for the 180 °C experiment. All ellipses reflect 2σ analytical uncertainties.

Deleted: 7

1561
1562

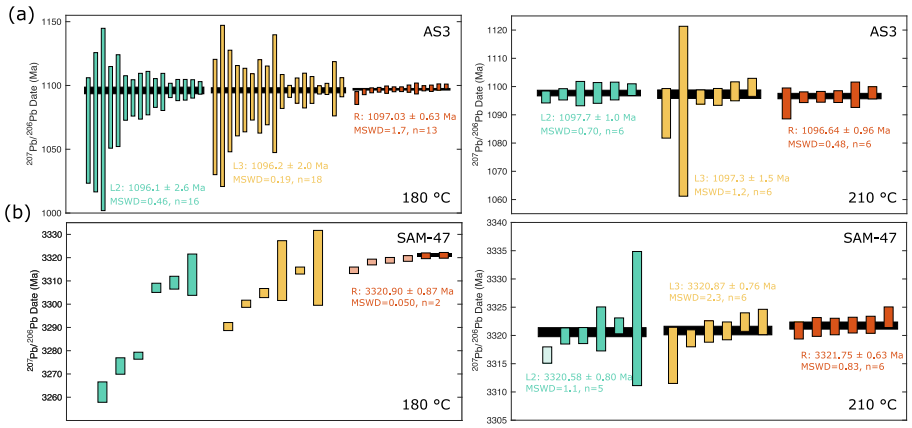

Figure 2. Ranked order $^{207}Pb/^{206}Pb$ dates for the **(a)** AS3 and **(b)** SAM-47 experiments. Black bars represent weighted means. Bar heights and quoted uncertainties reflect propagated 2σ analytical uncertainties.

Deleted: 8

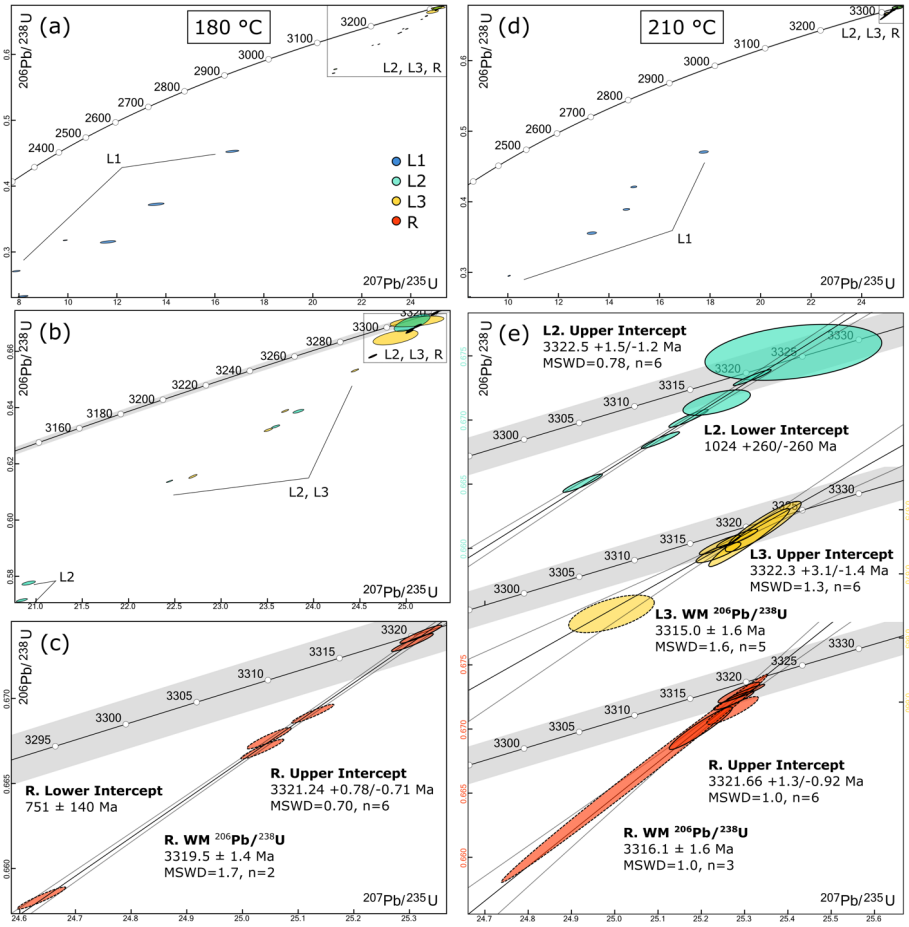

Figure 3. U-Pb concordia diagrams for the SAM-47 180 °C (left) and 210 °C (right) step-leaching experiments. **(a)** All data for the 180°C experiment. **(b)** Close up of the L2, L3, and R 180 °C dataset. **(c)** Close up of the 180 °C residue data. WM stands for weighted mean. **(d)** All data for the 210°C experiment. **(e)** Stacked plot showing the L2, L3, and R 210 °C datasets. All ellipses reflect 2σ analytical uncertainties. Dashed ellipses are excluded from weighted mean calculations.

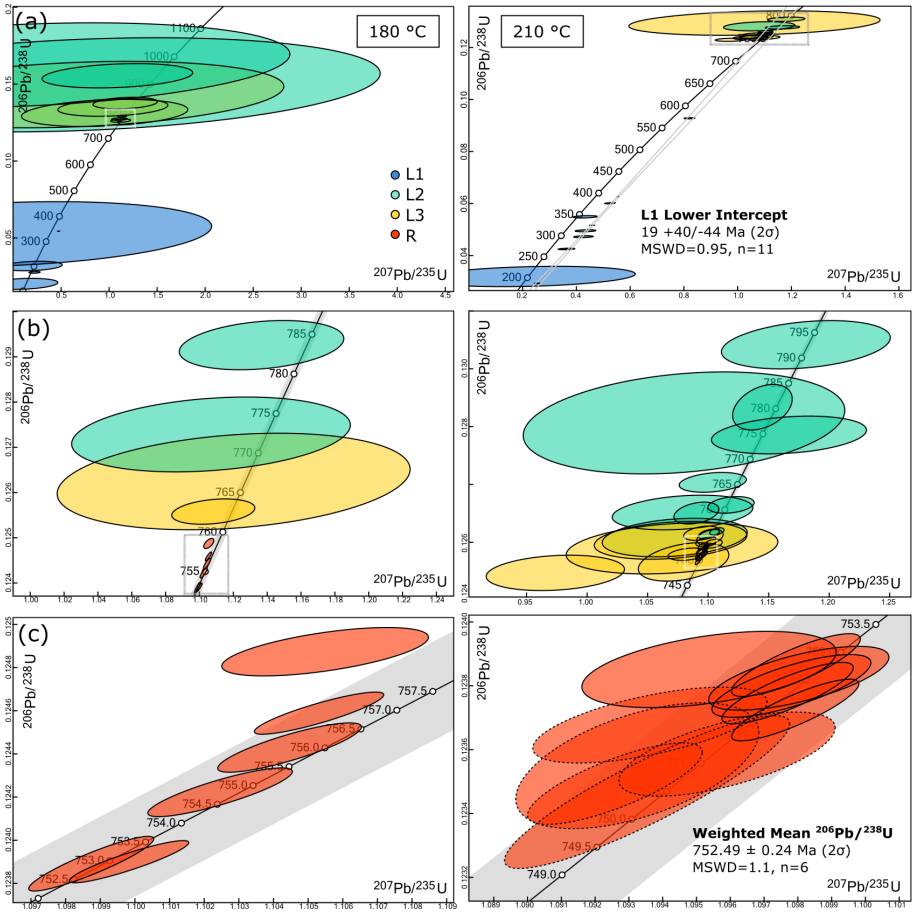

Figure 4. U-Pb concordia diagrams for the KR18-04 180 °C (left) and 210 °C (right) step-leaching experiments. **(a)** All data are depicted. **(b)** Close up of L2, L3, and R data excluding leachates with Pb^*/Pb_c values < 1. **(c)** Close up of zircon residues. The weighted mean $^{206}Pb/^{238}U$ date reported for the 210 °C experiment includes residue data with solid ellipse borders. Ellipses with dashed borders were excluded due to low-quality U measurements. All ellipses reflect 2σ analytical uncertainties.

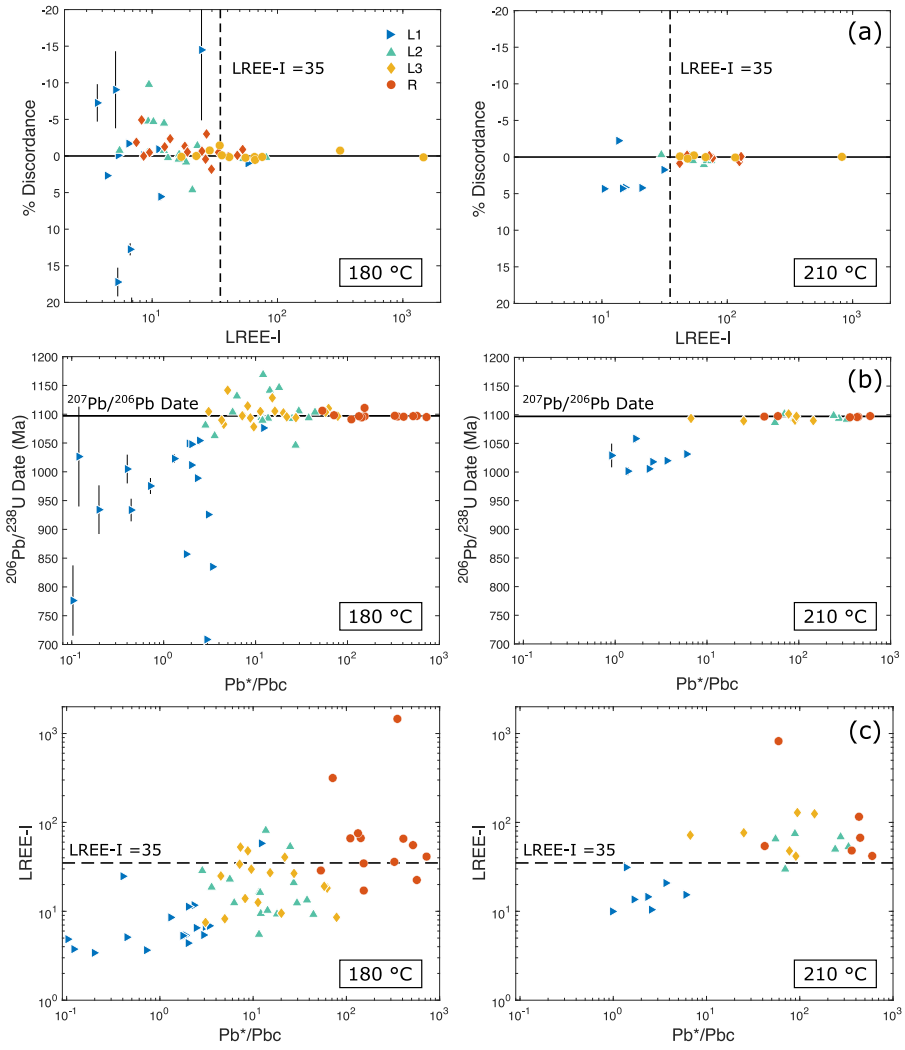

Figure 5. AS3 U-Pb and trace element data for the 180 °C (left) and 210 °C (right) experiments. **(a)** LREE-I versus percent discordance. The horizontal solid line represents perfect concordance. The vertical dashed line depicts a LREE-I threshold value of 35 below which data is notably more discordant. **(b)** ^{206}Pb/^{238}U date plotted as a function of the radiogenic Pb* to common Pb ratio. Error bars for the percent discordant and ^{206}Pb/^{238}U data reflect propagated 2σ analytical uncertainties. Most error bars are smaller than data markers. **(c)** The radiogenic Pb* to common Pb ratio versus the LREE-I showing a positive correlation between the two variables.

1571

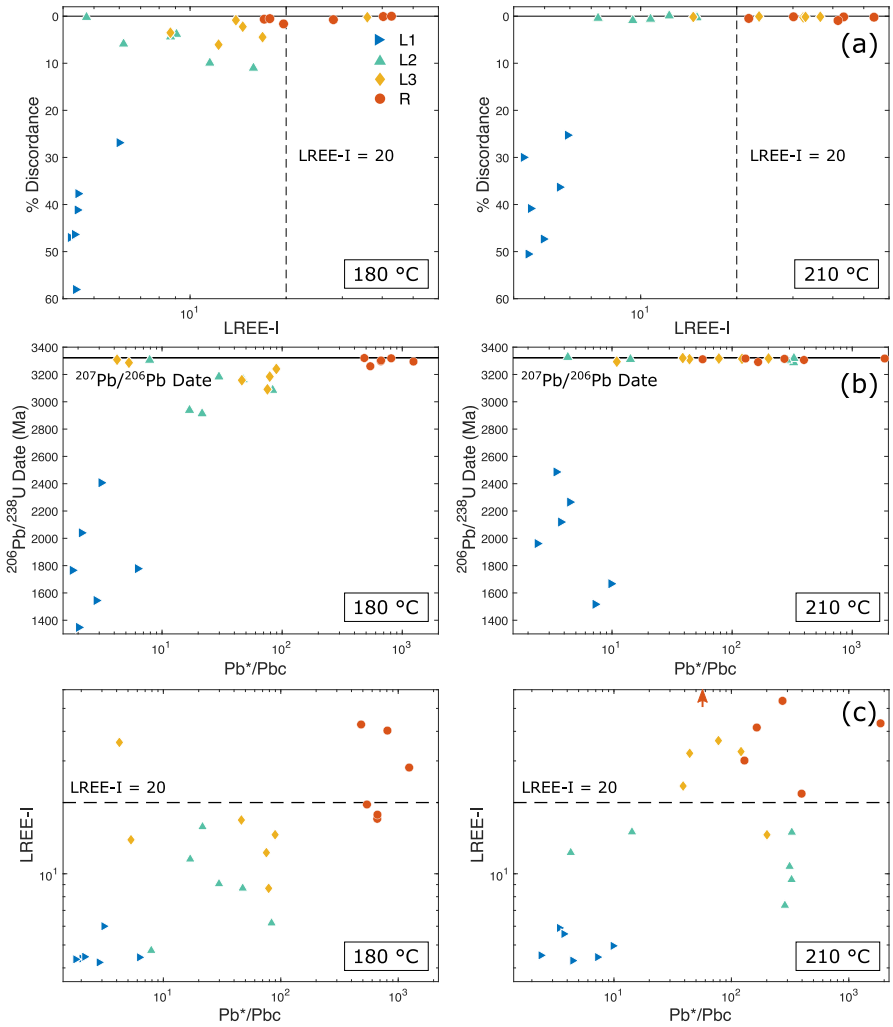

Figure 6. SAM-47 U-Pb and trace element data for the 180 °C (left) and 210 °C (right) experiments. **(a)** LREE-I versus percent discordance. The horizontal solid line represents perfect concordance. The vertical dashed line depicts a LREE-I threshold value of 20 below which data is notably more discordant. **(b)** ^{206}Pb/^{238}U date plotted as a function of the radiogenic Pb* to common Pb ratio. Error bars for the percent discordant and ^{206}Pb/^{238}U data reflect propagated 2σ analytical uncertainties. Most error bars are smaller than data markers. **(c)** The radiogenic Pb* to common Pb ratio versus the LREE-I showing a positive correlation between the two variables.

Deleted: ¶

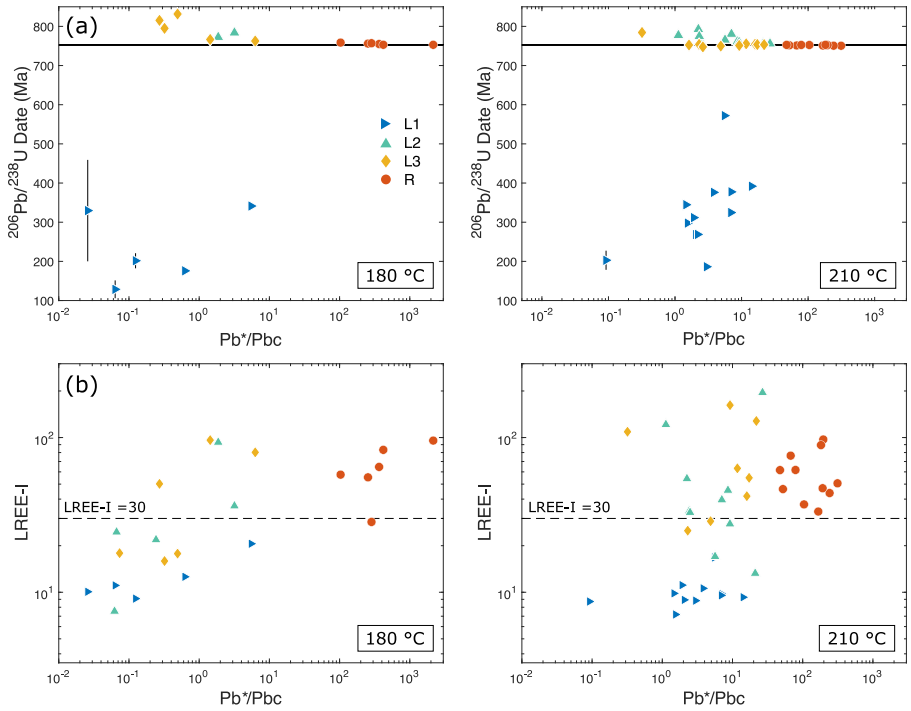

Figure 7. KR18-04 U-Pb and trace element data for the 180 °C (left) and 210 °C (right) experiments. **(a)** $^{206}Pb/^{238}U$ date plotted as a function of the radiogenic Pb* to common Pb ratio. 2σ analytical uncertainties for the percent discordant and $^{206}Pb/^{238}U$ data are smaller than data markers. **(b)** The radiogenic Pb* to common Pb ratio versus the LREE-I.

1575
1576
1577

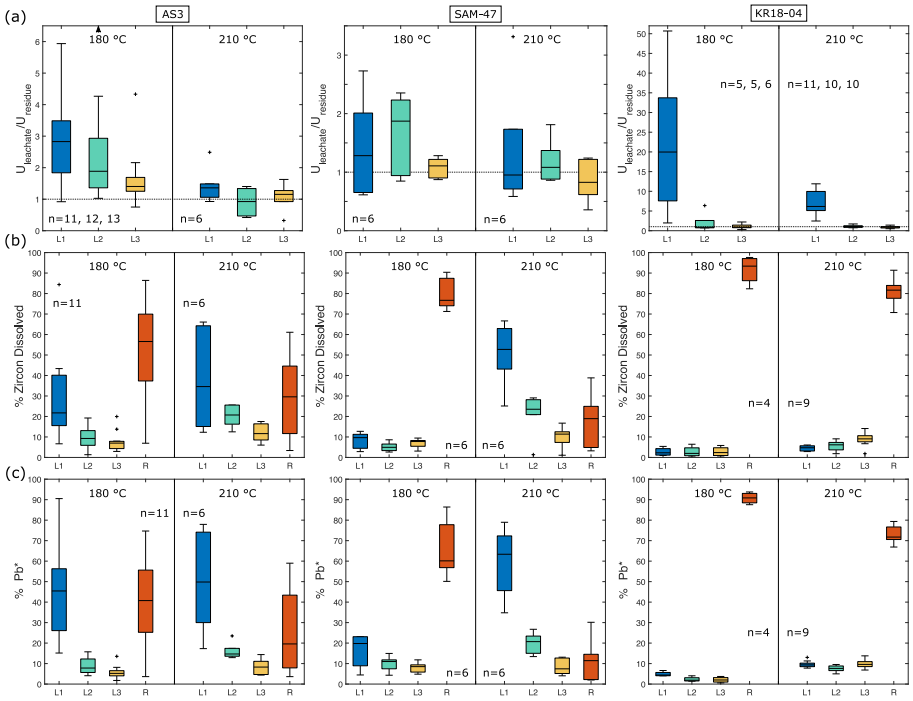

Figure 8. Box plot diagrams depicting geochemistry data for all step-leaching experiments. Each box shows the median value (black bar), the upper and lower quartiles (box), the minimum and maximum values (whiskers), and statistical outliers (plus marks) **(a)** Uranium concentration of leachates relative to that of their associated residue. **(b)** Percent zircon dissolved per leaching step based on measured Zr abundances. **(c)** Percent of radiogenic Pb measured per leaching step.

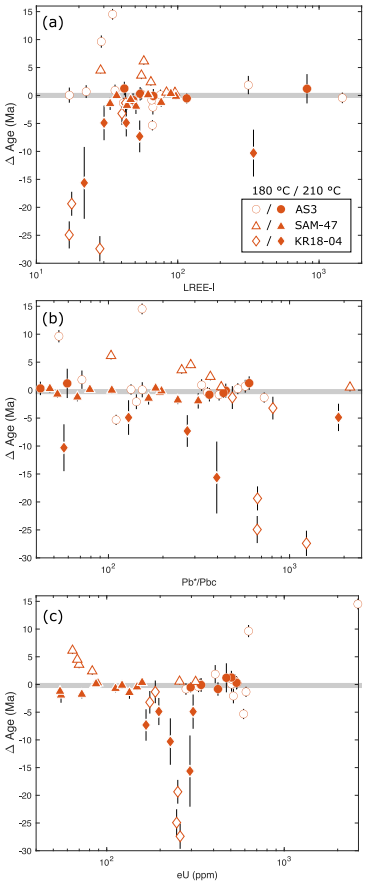

Figure 7. Trace element and Pb isotopic composition of zircon residues plotted against Δ Age as described in text. The gray bar at Δ Age = 0 Ma marks the accepted crystallization age for each zircon sample. **(a)** LREE-I versus the Δ Age. **(b)** Pb^*/Pb_c versus the Δ Age. **(c)** eU versus Δ Age. The arrow in each plot marks the placement of a datapoint from the SAM-47 dataset that plots at Δ Age = -60 Ma.

Deleted: 9

Deleted: The data portrayed is inclusive of residues from both the 180 °C and 210 °C experiments.

Formatted: Subscript

1580
1581

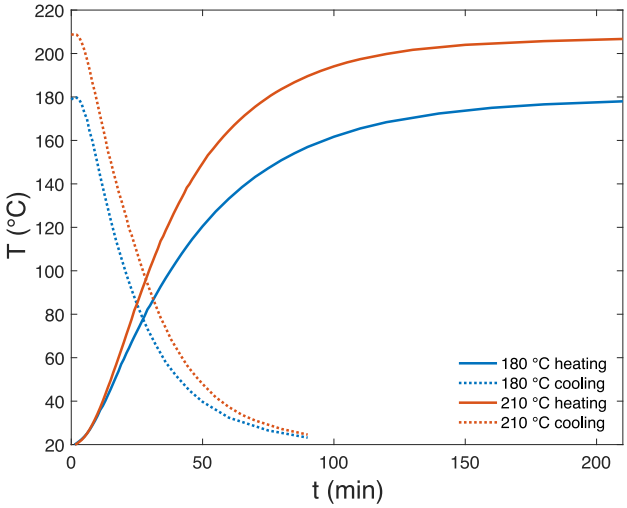

Figure 10. Temperature of the PTFE-lined pressure dissolution vessel plotted as a function of time. A fan was used to speed up cooling.

1582
1583
1584

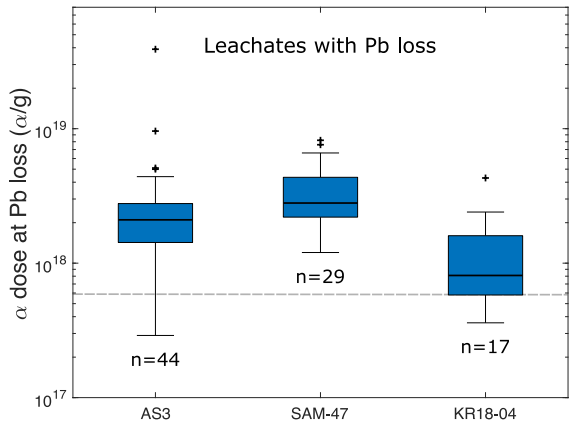

Figure 11. Box plot diagram showing alpha dose distribution for leachates (L1, L2, and L3) affected by Pb-loss. Data include both the 180 °C and 210 °C experiments. The gray dashed line highlights our best estimate for the minimum alpha dose required for Pb-loss to occur. Each box shows the median value (black bar), the upper and lower quartiles (box), the minimum and maximum values (whiskers), and statistical outliers (plus marks).

Deleted: Pb

Deleted:

1585
1586

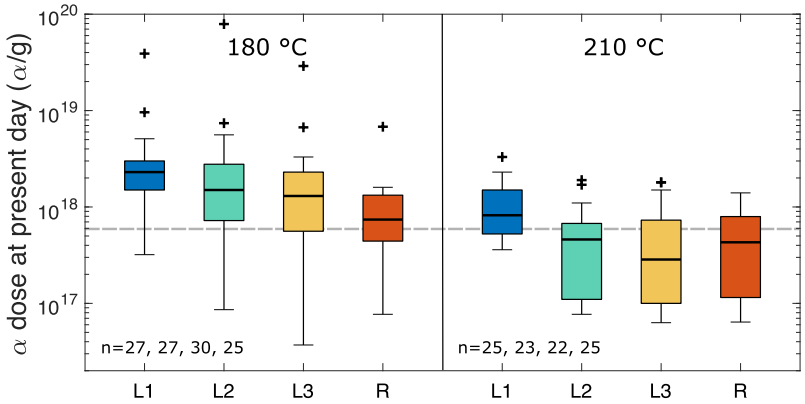

Figure 12. Box plot diagram showing present day alpha dose distributions at each step of zircon dissolution. Data includes all AS3, SAM-47 and KR18-04 leachates and residues. Alpha dose estimates reflect samples' present day radiation damage. The gray dashed line highlights our best estimate for the minimum alpha dose required for Pb-loss to occur. Each box shows the median value (black bar), the upper and lower quartiles (box), the minimum and maximum values (whiskers), and statistical outliers (plus marks).

Deleted: 10

Deleted:

1587
1588
1589

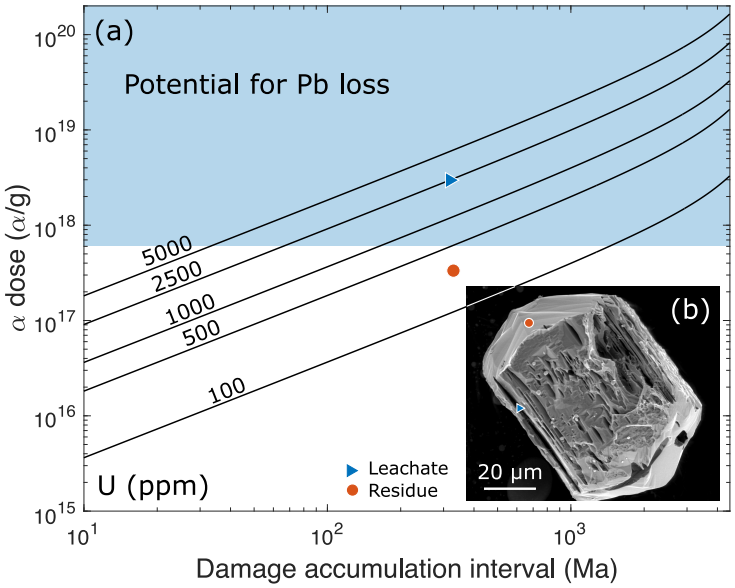

Figure 8. **(a)** Contour diagram showing alpha dose as a function of time for U concentrations ranging from 100 ppm to 5000 ppm. Calculations assume a fixed Th/U of 0.5 and no annealing. The shaded region highlights the alpha dose range in which Pb loss is most likely. **(b)** Secondary electron image of KR18-04 residue chemically abraded at 210 °C for 12 h from McKanna et al., (2023). The blue triangle marks a thin concentric zone that dissolved during chemical abrasion (leachate), while the red circle marks a portion of the zircon that remained intact (residue). Markers in b) correlate to markers in a) and illustrate how a grain with radionuclide zoning can have accumulated alpha doses above and below the threshold for Pb mobilization.

Deleted: 13

Table 1. Alpha dose estimates.

Sample	α dose (α/g)[1]						α_r dose (α/g)[2]	
	Total		Pb-Loss		Present Day		Present Day	
	Min	Max	Min	Max	Min	Max	Min	Max
AS3	4×10^{17}	1×10^{20}	3×10^{17}	8×10^{19}	3×10^{17}	8×10^{19}	2×10^{17}	$>1\times10^{19}$
SAM-47	2×10^{18}	1×10^{19}	1×10^{18}	8×10^{18}	3×10^{17}	2×10^{18}	6×10^{17}	2×10^{18}
KR18-04	1×10^{17}	1×10^{19}	4×10^{16}	4×10^{18}	4×10^{16}	4×10^{18}	5×10^{16}	7×10^{17}

[1]Calculated using measured U and Th concentrations and damage accumulation intervals as described in text.

[2]Raman-based alpha dose estimates reported by McKanna et al., (2023).

1593

Formatted: Indent: Left: 0.33", First line: 0"

Page 7: [1] Deleted Alyssa McKanna 10/6/23 1:38:00 PM

Page 7: [1] Deleted Alyssa McKanna 10/6/23 1:38:00 PM

Page 7: [1] Deleted Alyssa McKanna 10/6/23 1:38:00 PM

Page 7: [2] Deleted Alyssa McKanna 9/27/23 10:47:00 AM

Page 7: [2] Deleted Alyssa McKanna 9/27/23 10:47:00 AM

Page 7: [2] Deleted Alyssa McKanna 9/27/23 10:47:00 AM

Page 7: [2] Deleted Alyssa McKanna 9/27/23 10:47:00 AM

Page 7: [2] Deleted Alyssa McKanna 9/27/23 10:47:00 AM

Page 7: [2] Deleted Alyssa McKanna 9/27/23 10:47:00 AM

Page 7: [2] Deleted Alyssa McKanna 9/27/23 10:47:00 AM

Page 7: [2] Deleted Alyssa McKanna 9/27/23 10:47:00 AM

Page 7: [2] Deleted Alyssa McKanna 9/27/23 10:47:00 AM

Page 7: [2] Deleted Alyssa McKanna 9/27/23 10:47:00 AM

Page 7: [2] Deleted Alyssa McKanna 9/27/23 10:47:00 AM

Page 7: [3] Deleted Alyssa McKanna 10/6/23 1:42:00 PM

Page 7: [3] Deleted Alyssa McKanna 10/6/23 1:42:00 PM

Page 7: [3] Deleted Alyssa McKanna 10/6/23 1:42:00 PM

Page 7: [3] Deleted Alyssa McKanna 10/6/23 1:42:00 PM

Page 7: [3] Deleted Alyssa McKanna 10/6/23 1:42:00 PM

Page 7: [3] Deleted Alyssa McKanna 10/6/23 1:42:00 PM

Page 7: [3] Deleted Alyssa McKanna 10/6/23 1:42:00 PM

Page 7: [3] Deleted Alyssa McKanna 10/6/23 1:42:00 PM

Page 7: [4] Deleted Alyssa McKanna 9/27/23 11:08:00 AM

Page 7: [4] Deleted Alyssa McKanna 9/27/23 11:08:00 AM

Page 7: [4] Deleted Alyssa McKanna 9/27/23 11:08:00 AM

Page 7: [4] Deleted Alyssa McKanna 9/27/23 11:08:00 AM

Page 7: [4] Deleted Alyssa McKanna 9/27/23 11:08:00 AM

Page 7: [4] Deleted Alyssa McKanna 9/27/23 11:08:00 AM

Page 7: [4] Deleted Alyssa McKanna 9/27/23 11:08:00 AM

Page 7: [5] Deleted Alyssa McKanna 9/27/23 11:26:00 AM

Page 7: [5] Deleted Alyssa McKanna 9/27/23 11:26:00 AM

Page 7: [5] Deleted Alyssa McKanna 9/27/23 11:26:00 AM

Page 7: [5] Deleted Alyssa McKanna 9/27/23 11:26:00 AM

Page 7: [5] Deleted Alyssa McKanna 9/27/23 11:26:00 AM

Page 7: [5] Deleted Alyssa McKanna 9/27/23 11:26:00 AM

Page 7: [5] Deleted Alyssa McKanna 9/27/23 11:26:00 AM

Page 7: [5] Deleted Alyssa McKanna 9/27/23 11:26:00 AM

Page 7: [5] Deleted Alyssa McKanna 9/27/23 11:26:00 AM

Page 7: [5] Deleted Alyssa McKanna 9/27/23 11:26:00 AM

Page 7: [5] Deleted Alyssa McKanna 9/27/23 11:26:00 AM

Page 8: [6] Deleted Alyssa McKanna 9/27/23 10:28:00 AM

Page 8: [7] Deleted Alyssa McKanna 9/27/23 1:05:00 PM

Page 9: [8] Deleted Alyssa McKanna 10/3/23 1:24:00 PM

Page 9: [8] Deleted Alyssa McKanna 10/3/23 1:24:00 PM

Page 9: [8] Deleted Alyssa McKanna 10/3/23 1:24:00 PM

Page 9: [8] Deleted Alyssa McKanna 10/3/23 1:24:00 PM

Page 9: [8] Deleted Alyssa McKanna 10/3/23 1:24:00 PM

Page 9: [8] Deleted Alyssa McKanna 10/3/23 1:24:00 PM

Page 9: [8] Deleted Alyssa McKanna 10/3/23 1:24:00 PM

Page 9: [8] Deleted Alyssa McKanna 10/3/23 1:24:00 PM

Page 9: [8] Deleted Alyssa McKanna 10/3/23 1:24:00 PM

Page 9: [8] Deleted Alyssa McKanna 10/3/23 1:24:00 PM

Page 9: [9] Formatted Alyssa McKanna 10/2/23 10:21:00 AM

Font: Not Bold

Page 9: [9] Formatted Alyssa McKanna 10/2/23 10:21:00 AM

Font: Not Bold

Page 9: [10] Deleted Alyssa McKanna 10/2/23 10:14:00 AM

Page 9: [10] Deleted Alyssa McKanna 10/2/23 10:14:00 AM

Page 9: [10] Deleted Alyssa McKanna 10/2/23 10:14:00 AM

Page 9: [10] Deleted Alyssa McKanna 10/2/23 10:14:00 AM

Page 9: [10] Deleted Alyssa McKanna 10/2/23 10:14:00 AM

Page 9: [10] Deleted Alyssa McKanna 10/2/23 10:14:00 AM

Page 9: [10] Deleted Alyssa McKanna 10/2/23 10:14:00 AM

Page 9: [10] Deleted Alyssa McKanna 10/2/23 10:14:00 AM

Page 9: [10] Deleted Alyssa McKanna 10/2/23 10:14:00 AM

Page 9: [10] Deleted Alyssa McKanna 10/2/23 10:14:00 AM

Page 9: [10] Deleted Alyssa McKanna 10/2/23 10:14:00 AM

Page 9: [10] Deleted Alyssa McKanna 10/2/23 10:14:00 AM

Page 9: [10] Deleted **Alyssa McKanna** **10/2/23 10:14:00 AM**

Page 9: [10] Deleted **Alyssa McKanna** **10/2/23 10:14:00 AM**

Page 9: [10] Deleted **Alyssa McKanna** **10/2/23 10:14:00 AM**

Page 9: [10] Deleted **Alyssa McKanna** **10/2/23 10:14:00 AM**

Page 9: [10] Deleted **Alyssa McKanna** **10/2/23 10:14:00 AM**

Page 9: [10] Deleted **Alyssa McKanna** **10/2/23 10:14:00 AM**

Page 9: [10] Deleted **Alyssa McKanna** **10/2/23 10:14:00 AM**

Page 9: [10] Deleted **Alyssa McKanna** **10/2/23 10:14:00 AM**

Page 9: [10] Deleted **Alyssa McKanna** **10/2/23 10:14:00 AM**

Page 9: [10] Deleted **Alyssa McKanna** **10/2/23 10:14:00 AM**

Page 9: [10] Deleted **Alyssa McKanna** **10/2/23 10:14:00 AM**

Page 9: [10] Deleted **Alyssa McKanna** **10/2/23 10:14:00 AM**

Page 9: [10] Deleted **Alyssa McKanna** **10/2/23 10:14:00 AM**

Page 9: [10] Deleted **Alyssa McKanna** **10/2/23 10:14:00 AM**

Page 9: [11] Formatted **Alyssa McKanna** **10/2/23 11:03:00 AM**

Subscript

Page 9: [11] Formatted **Alyssa McKanna** **10/2/23 11:03:00 AM**

Subscript

Page 9: [12] Deleted **Alyssa McKanna** **10/2/23 11:03:00 AM**

Page 9: [12] Deleted **Alyssa McKanna** **10/2/23 11:03:00 AM**

Page 9: [12] Deleted **Alyssa McKanna** **10/2/23 11:03:00 AM**

Page 9: [13] Deleted **Alyssa McKanna** **10/3/23 9:44:00 AM**

Page 9: [13] Deleted **Alyssa McKanna** **10/3/23 9:44:00 AM**

Page 9: [14] Deleted **Alyssa McKanna** **10/6/23 2:01:00 PM**

Page 9: [14] Deleted **Alyssa McKanna** **10/6/23 2:01:00 PM**

Page 15: [15] Deleted **Alyssa McKanna** **10/3/23 11:18:00 AM**

Page 15: [16] Deleted **Alyssa McKanna** **10/12/23 12:03:00 PM**

Page 15: [17] Deleted **Alyssa McKanna** **10/3/23 11:22:00 AM**